Exploring the limits of foamed electrospun PCL fibers

Tutors: Suset Barroso Solares, Javier Pinto Sanz

Author: Borja García Marín

September 2020

Universidad de Valladolid

Máster en Física de Materiales

Abstract

Electrospinning, which is a technique capable of producing solid micro and nano fibers through the use of polymers solutions, have been used to produce polycaprolactone (PCL) fibers with different diameters. There are different parameters that influence the final characteristics of the fibers and, specifically, the relationship between the diameters of the fibers and the polymer concentration, the voltage, the flow rate, the distance needle-collector or the humidity have been studied. Furthermore, other techniques have been presented as possibilities to fabricate the hollow fibers, such as dry/melt/wet spinning and extrusion processes. Although those techniques are known nowadays and are used in practical applications, they did not allow producing hollow structures from fibers with a few micrometers of diameter or in the nanometer range. In this work a gas dissolution foaming path was followed, as it has been suggested previously, being an environmentally friendly and easy scalable technique. The fibers with different diameters have been subjected to a one-step gas dissolution foaming path, observing if the method allowed the fabrication of hollow fibers, and explore how the diameter of fibers influence the result. First, solid fibers from around 0.3 to 21 µm were obtained from electrospinning. Then, after the foaming procedure, it was found that fibers of a few micrometers presented hollow structures, while the smallest ones (close to 300nm) remained apparently intact. Moreover, the superficial morphology and the expansion ratio was studied, obtaining hollow fibers of 4 µm of diameter with superficial pores, and others, of about 20 µm of diameter, with an uniform solid skin.

Resumen

El electrospinning, una técnica capaz de producir micro y nanofibras sólidas mediante el uso de polímeros, se ha utilizado para producir fibras de policaprolactona (PCL) de diferentes diámetros. Hay diferentes parámetros que influyen en las características finales de las fibras y, específicamente, se ha estudiado la relación entre los diámetros de la fibra y la concentración del polímero, el voltaje, la velocidad de flujo, la distancia aguja-colector o la humedad. Además, otras técnicas se han presentado como posibilidades viables para fabricar fibras huecas, como los procesos de dry/melt/wet spinning y otros de extrusión. Aunque esas técnicas son conocidas hoy en día y se usan en la práctica para la producción de fibras, no permiten producir estructuras huecas con diámetros de unos pocos micrómetros o de rango nanométricos. En este trabajo se siguió una ruta, utilizada previamente con el mismo tipo de materiales, en la cual se aplica la técnica conocida como "gas dissolution foaming" sobre las fibras sólidas, siendo una técnica ecológica y fácil de escalar a grandes cantidades de muestras. Se ha utilizado la espumación "one-step" con el objetivo de observar si el método permitía la fabricación de fibras huecas, y explorar como influye el diámetro de las fibras en el resultado. Se obtuvieron fibras sólidas de alrededor de 0.3 a 21 µm mediante electrospinning. Mientras que las fibras de unos pocos micrómetros presentaron estructuras huecas después del gas dissolution foaming, las más pequeñas (cerca de 300nm) permanecieron aparentemente intactas. Además, se estudió la morfología superficial y el factor de expansión, obteniendo fibras huecas de aproximadamente 4 µm de diámetro con poros superficiales, y otras, con tamaños de 20 µm con una piel sólida uniforme.

1. Introduction

Electrospinning has become one of the most used techniques to generate polymeric-based nano and micro fibers[1]. This technique consists in applying a high voltage between a metallic needle attached to a syringe and a metallic collector. The syringe is filled with a polymer solution and placed into a syringe pump which controls the polymer solution flow rate. Furthermore, during the electrospinning process, the polymer solution presents induced charges on the outer surface of the liquid fed through the needle. The repulsion generated due to these charges induces the formation of "Taylor's cone", as well as the emission of a jet of material towards the collector[2]. In the trip needle-collector the solvent of the polymer solution evaporates, causing that polymer reaches the collector in a solid form. A proper processing parameters selection allows the polymer forming, an interlinked layer of solid fibers[3]. As a consequence, the fiber mats can be considered as tridimensional structures with a solid phase (i.e., the fibers), which could also show porosity on their surface, and a gaseous phase (i.e., the voids between fibers)[4]. In the Figure 1 is represented an electrospun setup scheme.
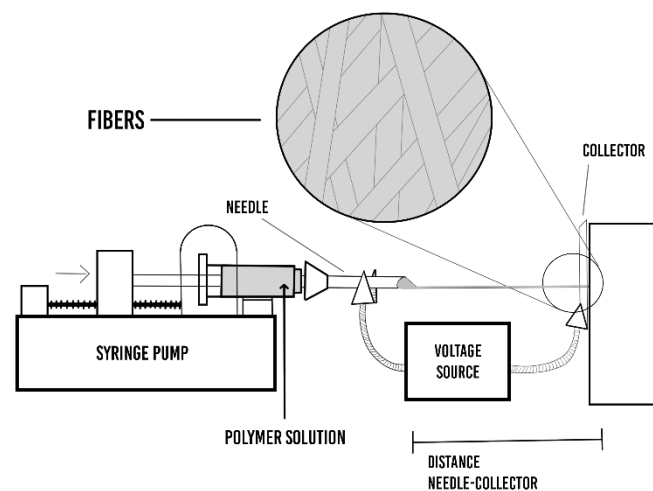

Figure 1 - Scheme of the electrospun setup used in this work.

A fine tuning on the processing parameters is a key issue to obtain electrospun polymeric fibers, or even to control their features[5–7], such as the fiber diameter, the absence of defects, the length of the fibers or the presence of surface porosity. On the one hand, some characteristics of the employed polymer solution have a remarkable influence on the obtained fibers: viscosity[8], filler concentration[9], conductivity[10], molecular weight[3], and surface tension[11]. On the other hand, several parameters are also fundamental on the production of fibers: voltage needle-collector[11–14], flow rate[15,16], distance needle-collector[17,18], needle-tip characteristics (length[12], diameter[19], coaxial[20,21]/simple[2,3,11]), and collector characteristics (fixed[9,10]/rotating[3]). The collector can be a rotating one, obtaining aligned solid fibers[3], or fixed, producing a random distribution of fibers[11,12]. Furthermore, environmental parameters like room temperature (RT)[19], room

3

humidity (RH)[4,22,23], and atmospheric pressure[15] could present an important influence in the proper evaporation of the solvent and, therefore, in the fiber formation.

One of the advantages of electrospinning is the capability of producing solid fibers using a wide selection of different materials[24], such as polymethylmethacrylate (PMMA)[1,10,25,26], polycaprolactone (PCL)[9,10], polyvinyl acetate (PVA)[11,27,28], polyvinylpyrrolidone (PVP)[19,20], polyvinylidene fluoride (PVDF)[3,12] and polyethylene terephthalate (PET)[9], among others. Moreover, this technique allows producing fibers from homogeneous polymers or polymer blends[1,9,25]. Furthermore, it is possible to add fillers, like nanoparticles of different natures[10], leading to different properties enhancement and functionalities. For example, C. Kuchi et al. [14] reported the optimization produced PVP fibers using TiO_2 as nanocomposite. It results functional in different fields such as photocatalysis, dye-sensitized solar cell (DSSC's), gas sensors, among others[19]. Moreover, Fe_3O_4 has been used to produce electrospun nanocomposite PCL fibers, providing advantages in controlled magnetic responsive antifungal drug release[29].

There are different applications where solid polymeric fibers can be employed, taking advantage of the diverse features that these materials can offer. The polymeric fibers can be used as a filter in separation process[5] e.g., by the addition of fillers to produce hydrophobic and oleophilic fibers capable of removing oil from water[10,25]. Also, by using proper materials, scaffolds with the required mechanical properties, biocompatibility, and biodegradation rate needed in biomedical applications (like drug delivery and tissue engineering)[2,9,28], can be produced by electrospinning. Specifically, PCL/PMMA blend fibers have been studied to be used in tissue engineering as fibrous scaffolds[1]. Moreover, polymeric fibers can be used as biosensors, as these materials present a larger effective surface area than bulk polymeric samples, being also stable in time and having accurate selectivity and sensitivity[5]. Furthermore, electrospun fibers can be used in other fields such as electronics (optoelectronics, photocatalysis, photovoltaics)[19], energy conversion (as separators or super capacitors)[30] and catalysis[5].

The versatility of the electrospinning technique generated a new research field, in which several modifications or optimizations have been studied to extend the applications of the electrospun polymeric fibers[15,29]. In particular, it can be highlighted the coaxial electrospinning, which consists of using a coaxial needle, formed by two concentric needles capable of feeding two different solutions, usually leading to fibers with a core-shell structure. Moreover, this technique, by a proper selection and subsequent removal of the core material, allows producing hollow fibers, in which the solid polymeric shell is surrounding a void core[15,29,31]. Other techniques can be used to produce this kind of fibers like dry/melt/wet spinning and, extrusion processes[21,32,33], but electrospinning-based processes usually allow obtaining thinner fibers[16].

Hollow fibers are of particular interest due to the enhanced properties, regarding solid fibers, provided by their hollow structure[31]. They can have better performance in applications such as thermal regulation, thermal insulation, moisture management, anti-dirt, or anti-static[34]. Also, other remarkable characteristics are their high surface-area-to-volume ratio, high loading capability (related to drug delivery), high surface reactivity and high permeability of the porous outer layer; which can be an advantage in the development of biomedical devices[34,35].

Recently, the CellMat Laboratory of the University of Valladolid (Spain) developed a new procedure to obtain hollow fibers from polymeric electrospun fibers, based on the gas dissolution foaming[36]. The gas dissolution foaming is an easily accessible, low cost, easy-scalable method, and environmentally friendly technique capable of producing bulk porous polymeric materials[37].

This foaming method can be explained in three phases. The first step consists on the polymer saturation; an autoclave is used to immerse a bulk material in a controlled high-pressure gas atmosphere, usually employing CO_2 or N_2[37–39]. The time required in the process must be long enough to allow the solid material reaching their maximum gas solubility at the selected saturation pressure and temperature. Then, once the maximum gas solubility has been reached, the pressure is released, starting the second stage of the foaming process. At this point, the quick pressure release induces a thermodynamic instability on the supersaturated polymer samples, which leads into the formation of nucleation points (air pockets) inside the solid. Then, the third stage (foaming) could happen almost simultaneously to the second (nucleation) if the working temperature is higher than the effective glass transition temperature of the polymer gas system (i.e., the solved gas acts as a plasticizer, decreasing the glass transition temperature), as the surrounding polymer chains possess enough mobility and the nucleation points can expand into pores. This is known as a one-step foaming process. On the contrary, if it is necessary to rise the temperature of the samples to overcome the effective glass transition of the polymer-gas system, usually by introducing the samples on a thermal bath (taking care of temperature and immersion time as a main parameters)[39], the procedure is called two-step foaming process. The gas dissolution method is used to generate nano and microcellular materials with high porosity, with numerous applications like thermal insulators or reducing the amount of weight trying to maintain the same structural properties[38]. In the Figure 2 is represented a gas dissolution foaming setup scheme.
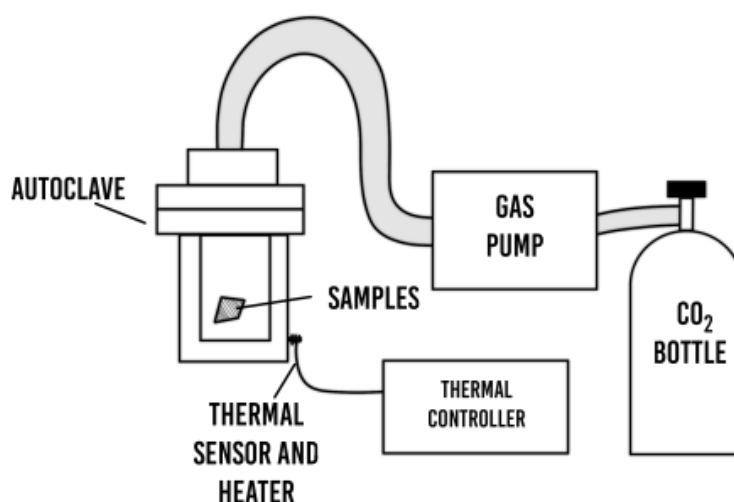
Figure 2 - Scheme of gas dissolution foaming setup used in this work.

Gas dissolution foaming has popularized as a technique to produce polymer foams, resulting in high porosity and low-density materials, being one of the last advances on this field the fabrication of nanoporous materials. Those materials have attracted a great interest due to their unique properties, such as their potential high thermal insulation behavior due to the Knudsen effect[40], and the possibility of producing transparent nanocellular structures, which has been reported using PMMA[41].

However, this technique presents a severe limitation in terms of the thickness of the sample, which must be at least on the millimeters scale to achieve satisfactory results. This is because

the gas quickly starts to diffuse out of the sample as soon as the pressure is released, usually losing the outer layers of the foamed samples (e.g., about hundreds of microns) most of the dissolved gas and therefore the capability to foam. Accordingly, the foaming of micro and nano materials has been hindered due to their dimensions (i.e., the expected solid external layer of hundreds of microns due to the loss of the dissolved gas is thicker than these samples). Nevertheless, in the last years it has been possible to overcome this limitation by the use of gas diffusion barriers around these materials that can be easily removed after foaming[42]. Following this approach, the researches of the CellMat Laboratory were capable to obtain the first generation of foamed hollow polymeric fibers from conventional solid electrospun polymeric fibers[36].

Herein, the limits and potential advantages of this new procedure to obtain hollow polymer fibers are explored. In particular, polycaprolactone (PCL) was selected to produce the solid fibers due to their good mechanical properties, biocompatibility, and biodegradability[1,43]. With this aim, PCL solid fibers with different diameters are produced by adjusting the production parameters of the electrospinning process. After obtaining the diverse solid fibers, they were imbibed in polyvinyl alcohol (PVOH), which was selected to act as the gas diffusion barrier. The imbibed fibers were subjected to the gas dissolution foaming procedure, using a time long enough to allow the complete saturation of the sample. The optimum saturation temperature was previously studied by Barroso-Solares et al.[36]. Accordingly, the morphology and structure of the solid and obtained foamed fibers, after removing the PVOH layer, were studied, by optical microscopy, scanning electron microscopy (SEM), and image analysis software[44,45]. Furthermore, differential scanning calorimetry (DSC) allows determining melting temperature, as well as the crystallinity of the material, among other properties. Finally, the obtained results were related to the processing parameters (from both electrospinning and foaming processes) to understand the processing-structure relationships and the applicability limits of this new procedure.

2. Materials and Method

2.1. Materials

Polycaprolactone (PCL, Mw ~ 80 00 g/mol) was purchased from (Sigma Aldrich, Spain). Chloroform (CHCl$_3$, Purity (CG) > 99.8%, ρ = 1.48 g cm^{-3} at 25) was received from (Sigma-Aldrich, Spain). Poly (vinyl alcohol) (PVOH) (Mowiflex C17) was gently provided by Kuraray and dissolved in distilled water.

2.2. Electrospun Fiber Fabrication

First, a proper amount of PCL was dissolved in CHCL$_3$ and left agitating at 800 rpm until the solution was completely homogeneous. The prepared solutions were 5, 7.5, 10, 15 and 17.5 wt.%, corresponding with 7.84, 12.1, 16.5, 26.3 and 31.6 mg/mL.

Then, 1 mL polymer solution was charged into a syringe equipped with a 21G needle and placed in a syringe pump (NE-1000, New Era Pump Systems, Inc.). The needle was introduced on a closed box at RT to prevent possible air-currents, environmental conditions changes, and accidental electrical discharges. A high voltage was applied between the needle and a copper sheet covered by an aluminum foil acting as a collector. A negative 2 kV voltage was fixed in the collector, while the variable positive one was applied in the needle with the aim of controlling

the effective voltage. The fibers were collected onto a copper plate covered with an aluminum foil. The voltage applied, the distance collector-needle, the flow rate and the polymer concentration were modified to optimize morphology of fibers, while the RH was tracked.

2.3. Gas Dissolution Foaming Process

Polyvinyl alcohol (PVOH) was dissolved in distilled deionized water (52 mg/mL). Then, this solution was casted over the fiber mats, imbibing them in a 300 µm layer of PVOH acting a gas diffusion barrier.

Then, samples of around 1 cm^2 of each imbibed solid fibers were subjected to the gas dissolution foaming method. An autoclave (PARR 4760 model) supplied by Parr Instrument Company (Moline, IL, USA), with CO_2 (medical-grade of carbon dioxide, 99.9% purity) pressure controlled by a gas pump (STF-10 model), was used for this process. Saturation pressure was set at 30 MPa, and temperature at 45 °C. Furthermore, the saturation time was 24 hours, to ensure reaching the maximum gas saturation of the polymeric fibers. The selected saturation parameters allowed the foaming of the solid fibers during the pressure release, without any additional heating (i.e., one-step foaming process).

Before further analysis, the PVOH layer from the fibers was removed. With this aim, after the fibers were taken out of the autoclave, they were introduced in an ultrasound deionized water bath at RT. The distilled water was changed each 15 minutes up to a total washing time of 60 minutes to ensure the complete elimination of the PVOH layer.

2.4. Fibers Characterization

Optical Microscope (Microscope DM2500 M, Leica; Camera, EC3, Leica) was used as a first approach to determine approximate size and homogeneity of fibers, while electrospun parameters were being optimized.

Once the optimal conditions were known, Scanning Electron Microscope (SEM, Hitachi, flexSEM1000) was used to study the diameter of fibers, as well as the morphology of the surface and cross-section. Furthermore, the SEM images were used to compare between the solid and hollow samples. The fiber mats were introduced in liquid nitrogen to allow fracturing the samples to expose the cross-section without deformation. Prior to the SEM observation, the fibers were coated by a 10 nm gold layer using a sputter coater (SDC 004 model, Balzers Union) step needed for non-conductor materials.

The fiber diameter distribution were obtained from the SEM micrographs using a specific software based on FIJI/ImageJ[44,45]. This program allows measuring individual fibers, and about a hundred fibers were randomly selected. Then, OriginPro was used to elaborate the distribution using data from ImageJ.

DSC was carried out using a differential scanning calorimeter. Furthermore, melting and crystallinity temperature were calculated. The thermal analyses were performed with a heating rate of 10.0 °C/min from -20 °C to 100 °C. After the first heating, samples were cooled until a complete solidification, and the heating process was repeated.

3. Results and discussion

3.1. Fabrication parameters

The electrospun parameters have been optimized towards the obtention of uniform fibers, trying to minimize the standard diameter distribution of samples. The final properties of fibers, like the diameter or the morphology will depend on the parameters utilized, so a fine tune of the electrospun conditions (the polymer and the solvent used, the concentration of the solution, and all the parameters mentioned in the introduction) must be carried out to obtain the fibers. On the one hand, it varies with the type of polymer used (the structure and adjacent molecular groups are relevant) and its molecular weight, while the selected solvent type also has a significant impact, influencing the way on how it evaporates. In this work, the PCL solution was used in different concentration with the aim to obtain fibers with different diameters. On the other hand, the rest of the parameters were adjusted following an optimization process that will be explained in the following sections.

Furthermore, depending on the concentration used, i.e., the solution viscosity, the parameters needed to carry out an appropriate electrospun process could be different. Specifically, the main three equipment electrospun parameters which are set were the voltage, the distance, and the flow rate, used in range of 15 to 25 kV, 15 to 20 cm, 0.2-1 mL/h, respectively. And the RH was tracked, varying between 25%-50%.

3.1.1. Flow rate

To start with, one of the most critical parameters in electrospinning is the flow rate. It must be fixed mainly depending on the solution viscosity, that is because it ensures the properly polymer flow, allowing the fiber formation[16]. If the flow rate is too high, it would be more polymer emerging out of the needle than the necessary to allow the formation of the Taylor's cone. This situation hampers the formation of uniform fibers, facilitating bead formation as it is shown in Figure 3. Furthermore, when the flow rate is too high, wet fibers were obtained, and other consequences could be observed, such as the presence of points where fibers got linked and irregular morphologies[46]. Beads are the principal structure indicating the failure occurring during electrospun process, modifying the properties of the surface of fibers. Additionally, the flow rate should be high enough to allow the fibers to be emitted fluently, since, if it is too low two possibilities can happen. One possibility is that the solvent could dry too fast emitting small beads. The other one is more extreme, causing blockages in the needle and avoiding the polymer to be emitted[5,7]. The flow rate was changed in each sample to avoid beads, and it is indicated in each image. The Voltage, the distance, and the humidity are explained in the below sections.

8

a) 5 wt.% 20 kV 20 cm 0.3 mL/h 35 %RH   **b)** 5 wt.% 15 kV 15 cm 0.3 mL/h 42 %RT
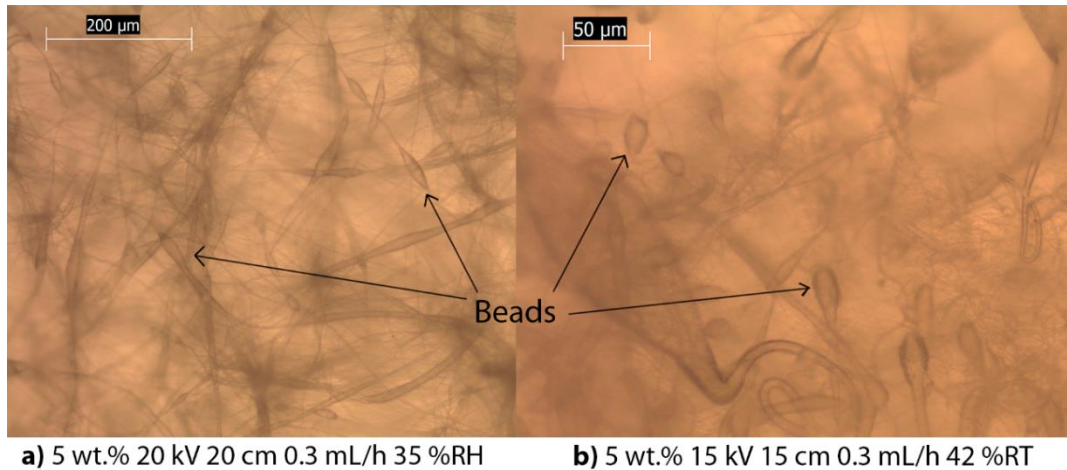
Figure 3 – Optic Microscopy images of Electrospun solid 5 wt.% PCL fibers at a) 20 kV and 20 cm, b) 15 kV and 15 cm needle-collector voltage and distance, respectively. Both are generated at 0.3mL/h. Beads can be appreciated in both pictures.

In this work two different situations were found (both comparation represented on Figure 4). On the one hand, for the low polymeric concentration solutions (5 wt.% and 7.5 wt.%), the excess flow rate produced beads and irregular wet fibers. The interconnexion of fibers are shown in Figure 4a, those were originated from the wet fibers, which arrived at the collector without a complete evaporation of the solution, and they got stick themselves. The aim of the electrospun process in this work is producing single and uniform fibers, so interconnexion and beads are undesirable, that is why low flow rates are preferable. On the other hand, for higher polymer concentration (10 wt.% to 17.5 wt.%) no beads formation was detected for higher flow

a) 7.5 wt.% 20 kV 15 cm 0.5 mL/h 38 %RH   **b)** 7.5 wt.% 20 kV 15 cm 0.3 mL/h 35 %RH

c) 15 wt.% 20 kV 20 cm 1.0 mL/h 30 %RH   **d)** 15 wt.% 20 kV 20 cm 0.8 mL/h 30 %RH
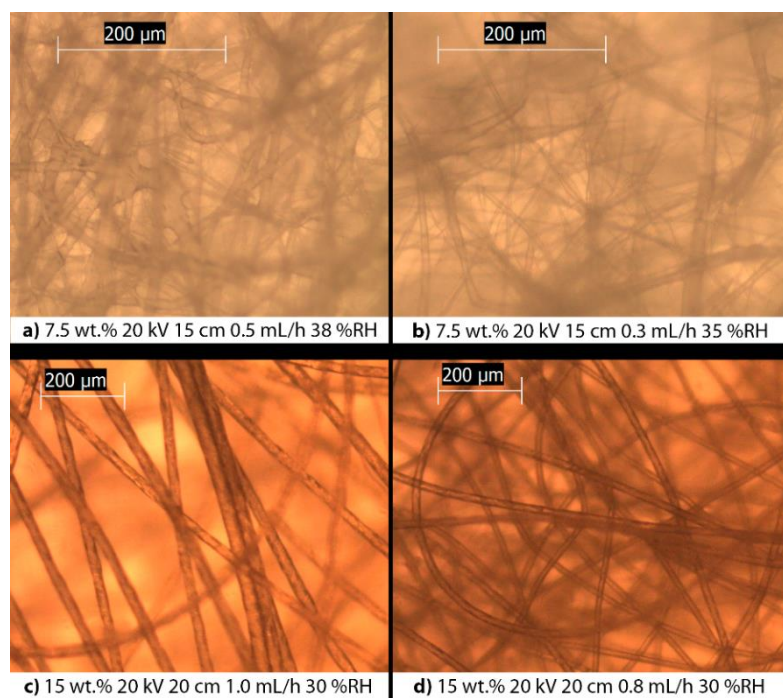
Figure 4 – Two different comparation of optic microscopy images of: electrospun solid 7.5 wt.% fibers at 20 kV 15 cm and around 35 %RH a) 0.5 mL/h and b) 0.3 mL/h; and 15 wt.% samples at 20 kV 20 cm 30 %RH c) 1 mL/h d) 0.8 mL/h. In first comparation more uniform fibers are produced while decreasing the flow rate. In the second, a slight decrease on fiber diameter has been observed.

rates. Instead, for high flow rates, fibers of different diameters were produced due to the excess of polymer in the Taylor's cone, while when the flow rate is decreased thinner fibers and homogeneous samples appeared (represented on Figure 4c and 4d). That was because if the flow rate was lower, there were no excess of the polymer in the formation of the Taylor's cone, so less irregularities were originated. These differences caused that the flow rate used for 5 wt.% and 7.5 wt.% was close to 0.2-0.3 mL/min, and for the other concentrations close to 0.6-0.8mL/h.

3.1.2. Voltage

The voltage is in charge of inducing electric charges in the polymeric solution. These charges are essential because they are the responsible for electric repulsion that cause the whole electrospun process[11,29]. Consequently, the charges will repel themselves, so if enough voltage is applied a polymer jet would form from the needle and directed to the collector (which is usually set with an opposite voltage to the needle). The voltage must be high enough to allow the Taylor's cone formation and it should be capable of overcome the superficial tension, otherwise, the fibers cannot form. In a typical electrospun process the voltage used can vary between 5 and 30 kV[5]. The voltage explored in this work was between 15-25kV. The minimum was set because no fibers were obtained under 15 kV using PCL and the highest value due to the electrospun setup limitations. Inside that range the polymer chosen formed a stable Taylor's cone. In general electrospun processes, if the voltage increases, the charges induced can increase the repulsive force in the needle, stretching the jet. As a consequence, on a first stage, a rise in voltage will induce a decrease on the diameter of the fibers[7]. Nonetheless, when the voltage is high enough (the umbral value depends on solution properties) the radial component in the repulsion force will be relevant, causing the fibers to expand and finally obtaining a higher diameter samples[5]. However, the diameter has a low dependence with the voltage as the electrospun repulsion force is high and it is difficult to perturb it.

The effect of voltage on the diameter of the fibers was mainly studied using 15 and 20kV. In Figure 5, it is possible to observe a comparison of the different gathered samples, which were obtained using the electrospun parameters displayed in the pictures such that it is easy to discern the differences caused by voltage variations. The samples from 7.5 wt.% (Figure 5a, 5b) and 10 wt.% (Figure 5c, 5d) have been produced in the same conditions (except the voltage), and a slight variation in the RH (not statistically significant). As expected, it was found that when the voltage increased the diameter of the fibers decreased in both samples. Furthermore, this effect cannot be observed on the 5 wt.% samples produced on this work, probably because the voltage variation is not high enough. The thinner fibers already had small polymer jet, so the difference of the voltage used to control the diameter must be higher. Meanwhile, for higher polymer concentrations (15 and 17.5 wt.%), it had only been used 20 kV, because of the homogeneous fibers were apparently obtained on an easier way. The selection of voltage used for late foaming investigation did not depend on the quantity of beads production, because change in voltage did not affect the bead formation in this work. Instead, the values utilized were those which produced the samples with more narrow distributions of diameters. Most cases, the samples selected were obtained from 20 kV electrospun procedures.
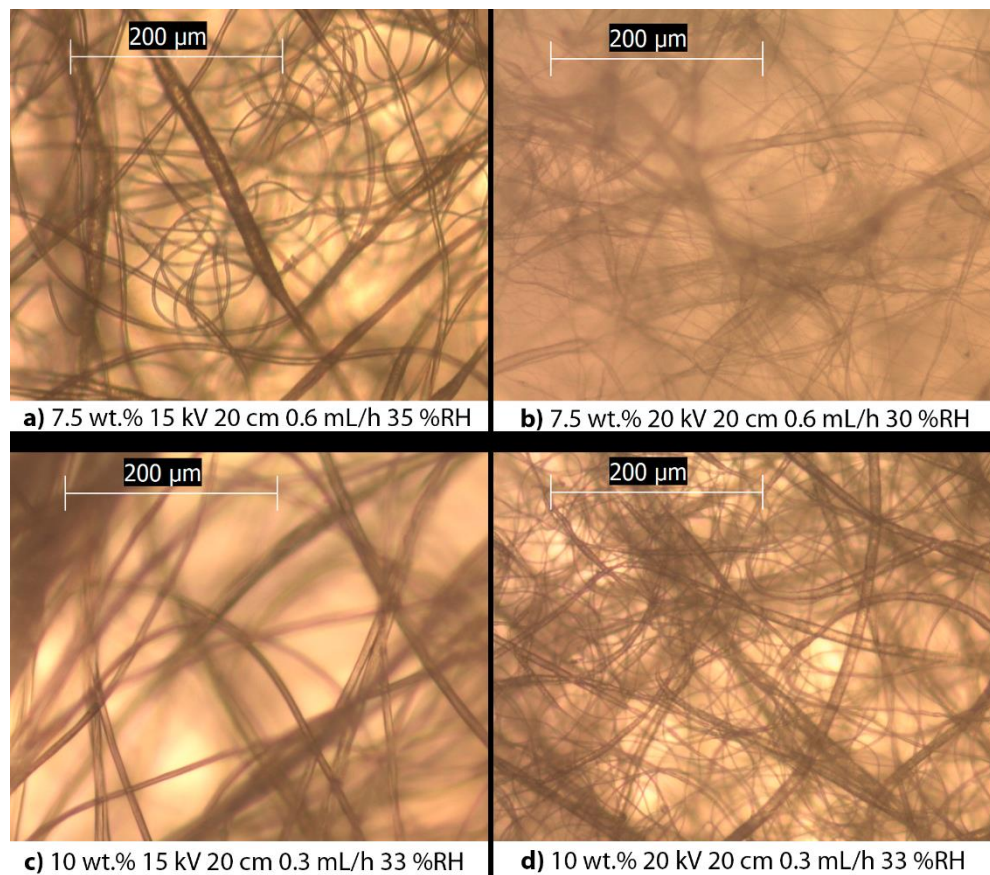
Figure 5 – Two different voltage comparatives are represented, both from optic microscopy images. Electrospun solid of topside consist on 7.5 wt.% 20 cm 0.6 mL/h 35 %RH (a, b) and downside on 10 wt.% 20 cm 0.3 mL/h 33 %RH (c, d). Left-side images were producing with 15 kV (a, c) and right-side samples with 20 kV (b, d). In both samples can be observed a decrease in fiber diameter, but the effect is less notable on first case.

The results obtained in this work agreed with the ones reported by Eleyas et al.[13], and they have observed a slightly decrease in the fiber diameter using polyacrylonitrile (PAN)[13]. They demonstrate that it is possible to control diameter and morphology of the electrospun fibers varying the voltage in nanometer range. A similar result was published by Yongyi et al., using Polysulfone (PSU) fibers[17] in a PSU/DMAc 10 wt.%, varying voltage from 27.5 kV to 45 kV resulting in a decrease of 250 nm to 150 nm. Other works, such as the work carried out of Bakar et al., whose use PAN as the electrospun material, and report on first place a decrease of the diameters, and then an increase for higher voltage[14]. In all works, as like in this one, other electrospun parameters are kept constant to study the voltage influence. Despite using different polymers for producing the fibers, the results are comparable to those obtained in this work, because physic explication behind the process is the same. Although different polymers may have distinct dependences, but the usual polymers react by the charges induced by the voltage.

3.1.3.   Needle-Collector Distance

The other main parameter of electrospinning is the distance between the needle and the collector, it is related with the disponible solvent evaporation time[12]. If the distance is low, the solvent will not be able to evaporate properly and it will cause irregularities on the morphology.

When the distance decreases is recommendable to decrease the flow rate, because the solvent to evaporate would be reduced as well[7]. But when the distance increases, the change can induce multiple different effects entering in conflict. On the one hand, if the distance increases, the time evaporation increases, and that induces tensions which make thinner fibers[5,7]. On the other hand, if the voltage is keep constant while the distance increases, the effective electric field decreases, resulting in a lower acceleration in the fiber emission process and facilitating the production of thicker fibers[5]. Therefore, the influence of this parameter will depend on the equilibrium of both effects.

Experimentally, the increase of the distance showed an effect on the $CHCl_3$ drying time. In Figure 6, there are represented the two cases that have been observed. First, for the lower concentration (5 wt.%), there was not a remarkable difference due to the presence of beads in both cases, but the singular fibers with higher diameter appear more frequently at low distances, because of the reduced time available for the solvent to evaporate (Figures 6a and 6b). Then, when the 10 wt.% solution was used, if the distance was reduced, wet fibers were produced again (Figure 6c). Consequently, a minimum of the distance is required to allow the

a) 5 wt.% 20 kV 15 cm 0.2 mL/h 44 %RH	b) 5 wt.% 20 kV 20 cm 0.2 mL/h 44 %RH
c) 10 wt.% 20 kV 15 cm 0.7 mL/h 30 %RH	d) 10 wt.% 20 kV 20 cm 0.7 mL/h 30 %RH
e) 17.5 wt.% 20 kV 15 cm 0.8 mL/h 35 %RH	f) 17.5 wt.% 20 kV 20 cm 0.8 mL/h 35 %RH
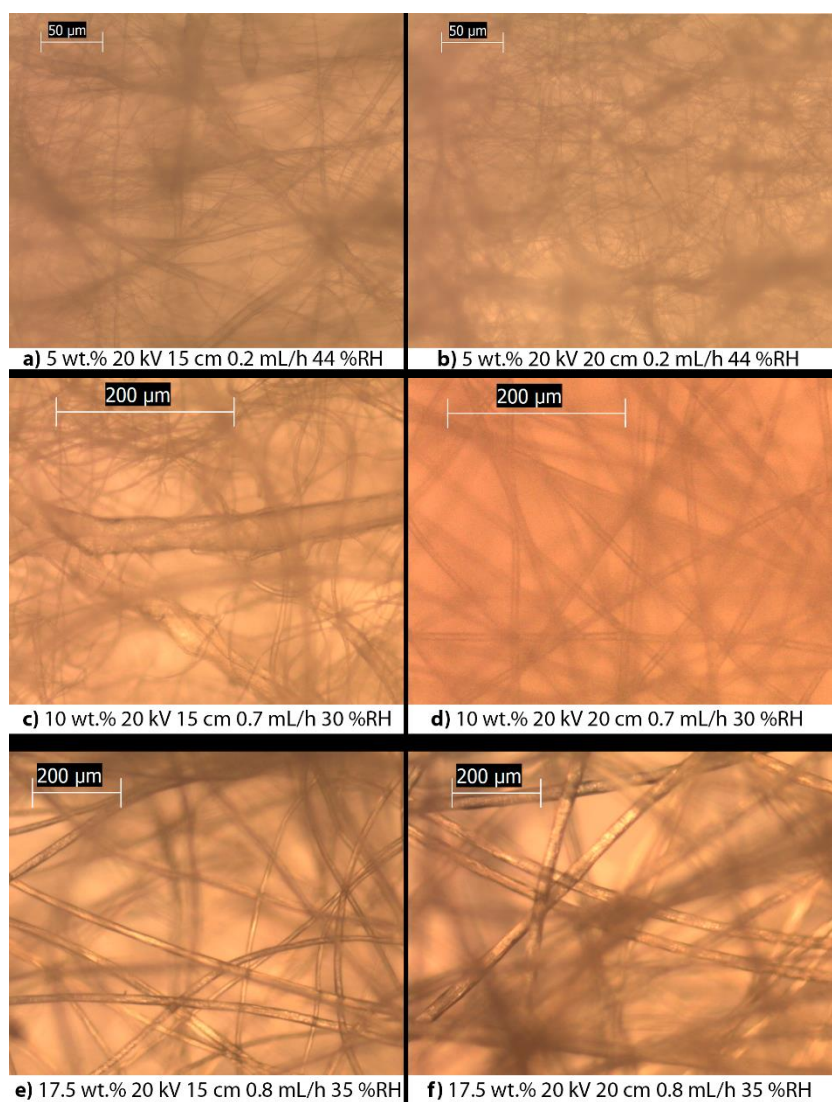
Figure 6 – Three different distance comparatives are represented, all from optic microscopy images. Electrospun solid of topside consists of 5 wt.% 20kV 0.2mL/h 44 %RH (a, b);the middle example, on 10 wt.% 20 kV 0.7 mL/h 30 %RH (c, d); and downside on 17.5 wt.% 20 kV 0.8 mL/h 30 %RH (e, f). Left-side images were producing with 15 cm (a, c, e) and right-side samples with 20 cm (b, d, f). In first comparation can be observed how irregular fibers change to regular ones, while in the second case an increase in diameter is observed.

complete solvent evaporation, as can be seen in Figure 6d, where uniform fibers can be appreciated. Moreover, for thicker fibers no beads or wet fibers were observed, instead, it affected to the diameter of the samples. For example, for the 17.5 wt.% samples, a decrease in sizes was induced by an increase of the distance (Figures 6e and 6f). In these cases, it is assumed that the effect from reducing the voltage was predominant, and the instabilities from higher evaporation time were not enough relevant. For the 15 wt.% cases, there was not observed a dependence between the flow rate and the diameter in samples, so it was assumed that the both effects explained above maintain an equilibrium at this specific conditions. However, it could be a slightly variation on the diameter of the fibers which needs further investigation, for example, varying the voltage in a proportionally quantity.

Jaruayporn et al. reported a variation of the electrospun fiber structure while changing the needle-collector distance. When the distance was too short, it was observed bead formation and the wet thick fibers on the collector[17,18]. But if the distance was increased not only the bead formation was reduced but also thinner fibers were reported using PSU[18]. In the above-mentioned work, the predominant effect was the drying-solvent one as thinner fibers were measured. The comparation between this work and the last-commented one shows how the different polymers may act different, and the study of each system must be study to know the relationship between the distance and the diameter of the fibers.

As a result, two different distances, 15 and 20 cm, were selected to produce different samples of each polymer concentration, with the aim to increase the variety of samples utilized on the gas dissolution foaming path. In all cases the flow rate used was not the same for both distances, the flow rate used samples with distances of 15 cm was lower than the used for 20 cm in all cases. Furthermore, the voltage was varied to obtain the more homogeneous samples possible.

3.1.4.   Humidity

Due to the influence of the environmental parameters on the final properties of samples, they must be taken in account. Specifically, the one which varied along the production of the fibers was the RH. It affects to the solvent evaporation, influencing on a different way depending if the solvent used is hydrophobic or hydrophile. In general, high RH facilitate the formation of thinner and longer fibers, involving distributions with different diameter of the fibers[7]. Consequently, this generates fibers of different sizes, producing double distributions of diameters. Moreover, a portion of the charges from the jet is discharged to the water molecules in the air, so for low RH, the charge density will be high in the jet. These instabilities generate breakages in the fibers, avoiding the production of longer fibers and facilitating instabilities[4]. Specifically, chloroform is a hydrophobic solvent, so in presence of high RH it will difficult the evaporation and resulted in superficial pores on the fibers. The presence of surface pores at high RH was hypothesized to be caused by the vapor-inducing a phase separation, where the chloroform remained in the fiber surface[4].

Figure 7 demonstrate the effect of humidity on the PCL/CHCl$_3$ combination, specifically, in the distribution of the diameters, which consist on the different images obtained in this work. Those have been fabricated under the same electrospun conditions but changing RH between 30 and 45% RH. It can be observed that when RH is increased, small fibers appeared, inducing a wider and more bimodal distribution. However, the fibers did not vary along their length, i.e., they were uniform. Similar results have been reported by Ramprasathhet al.[22], in which the fiber diameter decreased while the RH increase. However, in that work it is not found a doble

distribution, simply, the diameter is reduced. The proposed explanation is that as chloroform is a non-miscible-water solvent, so it could form a shield around the fiber, avoiding the water molecules getting close to the jet. As Roya et al.[4] proposed for the low RH situations, where charge dissipation did not occurred inducing instabilities and breakages, where the low diameter fibers could be produced. They did not predict this effect because the PCL was solved in chloroform/DSM 80/20%, and due to hydrophobic properties of DMF, the water molecules had easier to allow the charge dissipation.
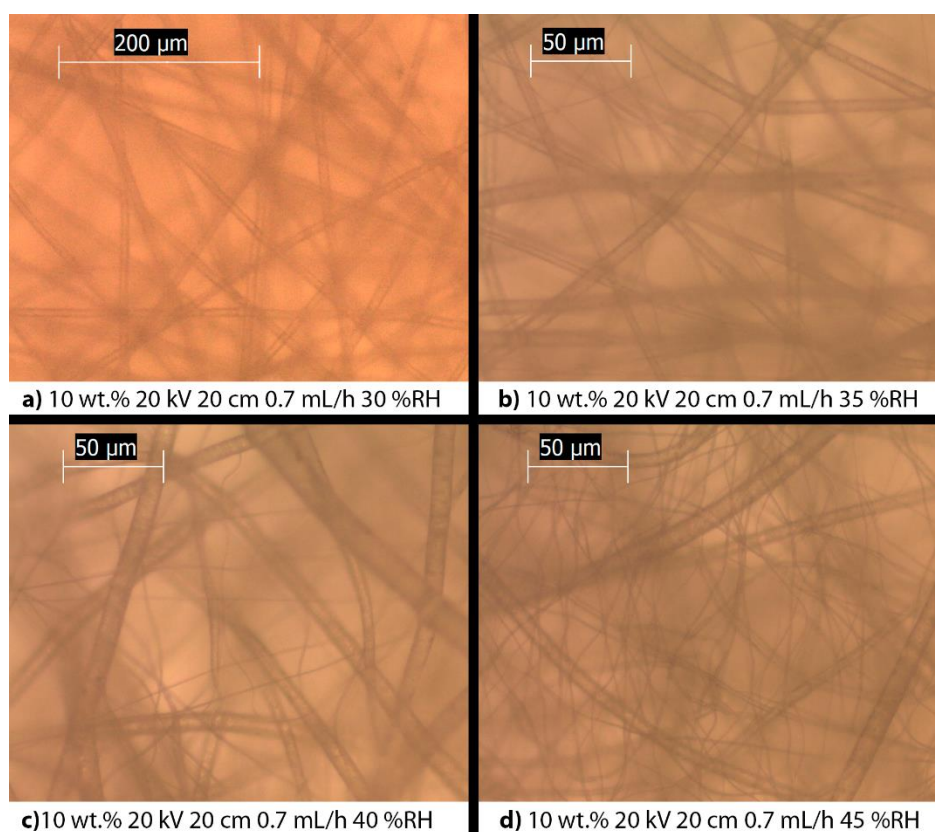
Figure 7 – Optic Microscopy images of electrospun solid 10 wt.% PCL fibers at 20 kV needle-collector voltage, 20 cm distance and a flow rate of 0.7 mL/h. The humidity used was a) 30 %RH b) 35 %RH c) 40 % d) 45 %RH. The evolution until a double distribution and the creation of thinner fibers is observed while RH increases.

Meanwhile, for low polymer concentrations thinner fibers were obtained, for instance, using 5 wt.%, fibers with diameters of hundreds of nanometers were obtained. In low RH samples wet fibers were observed, it could be associated with a unproperly $CHCl_3$ evaporation. This effect could not happen to other concentrations because the amount of solvent in higher concentration solutions is lower and could evaporate completely even at low RH. As high humidity seems to facilitate thinner fibers, double distributions were not favorable while RH is increased, however, more uniform fibers were produced (Figure 8). In this work was found that high RH (45 − 50 wt.%) was recommendable with low PCL concentration (5 − 7.5 wt.%), and lower RH (30 − 35 wt.%) induces more homogeneous samples of higher polymeric concentration(10 − 17.5 wt.%).

a) 5 wt.% 20 kV 15 cm 0.2 mL/h 35 %RH   **b)** 5 wt.% 20 kV 15 cm 0.2 mL/h 44 %RH
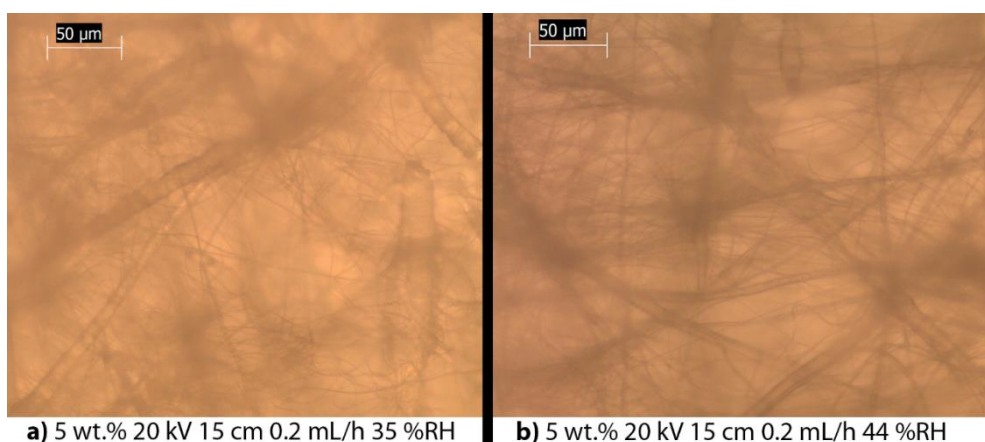
Figure 8 – Optic Microscopy images of electrospun solid 5 wt.% PCL fibers at 20 kV needle-collector voltage, 15 cm distance and a flow rate of 0.2 mL/h. The humidity used was a) 35 %RH b) 44 %RH. Irregular fibers are shown in low-humidity cases, and smoother one in higher RH.

Additionally, significant differences were found in the superficial morphology of the fibers, in Figure 9, it is easy to observe the increase of the superficial irregularities. Other works as Roya et al.[4], had reported porous micro-diameter fibers using PCL with the RH higher than 50 %. Whereas they found different behaviors to the use of the different solvent properties. In case that the solvent used is a quick-evaporating one, the pores were formed on the surface. If a water-miscible solvent is used, electrospinning produced fibers with irregular surface pores. On the contrary, non-water-miscible or hydrophobic ones allows formation of circular pores. The range of RH used in this work do not allow the pores formation, but it can be observed a evolution of longitudinal indents. As last consequence, for the 15 wt.% samples, it has been observed a small increase on the diameter of the fibers with the rise of RH, but this effect has not been observed for lower polymer concentration solution. The same effect has been

a)15 wt.% 20 kV 20 cm 0.8 mL/h 30 %RH   **b)**15 wt.% 20 kV 20 cm 0.8 mL/h 35 %RH

c)15 wt.% 20 kV 20 cm 0.8 mL/h 40 %RH   **d)**15 wt.% 20 kV 20 cm 0.8 mL/h 45 %RH
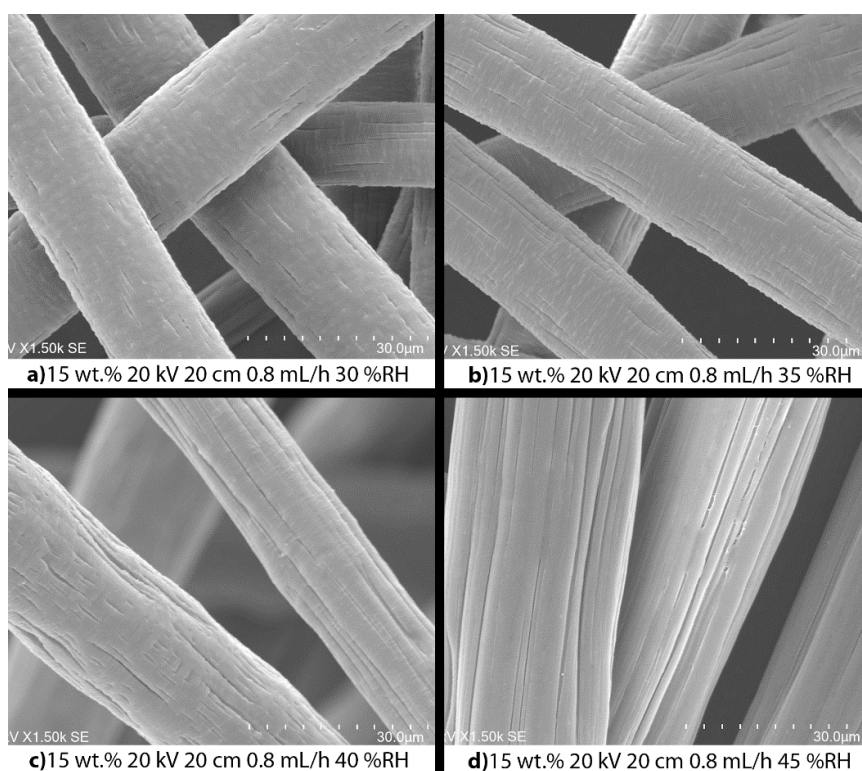
Figure 9– SEM images of electrospun solid 15 wt.% PCL fibers at 20 kV needle-collector voltage, 20 cm distance and a flow rate of 0.8 ml/h. The humidity used was a) 30% b) 35% c) 40% d) 45% RH. The apparition of longitudinal indents was observed by the increase of RH.

observed by Liwei et al.[23] using a PAN/DMF solution, which is a hydrophilic solvent, so it suggest that the diameter increase does not depend on the water-miscibility of the solvent. Nevertheless, these works did not report a double distribution in the fibers, the standard deviation of this works kept constant in single distribution while increasing the RH.

3.2. Optimized Fibers

Finally, most electrospun process were optimized keeping an equilibrium between the parameters, obtaining homogeneous samples. However, the cases where 5 and 7.5 wt.% polymer concentration were used, there were not completely optimized. Possibly the rate between the distance, the flow rate and the humidity did not allow the properly solvent evaporation, inducing some fibers various times larger than the others. In the Table 1 are resumed all the conditions of the solid fibers obtained after optimizing the different parameters mentioned above for each polymer concentration, and a surface image with the distribution of diameters are represented in Figure 10. Apart from bibliography[19,20], the SEM observations of the foamed fiber samples confirmed the possibility of the gas dissolution path of foaming. Criteria followed to the fiber selection is explained in this paragraph. On the first place, it has been required for the samples the absence of beads. Then, the uniform fibers are preferable, i.e., the diameter of each fiber cannot vary significantly along its length. Lastly, the third requirement established was related with homogeneity, i.e., minimize the diameter standard normalized deviation. This is because each sample should consist on a single diameter size to improve the data analysis accuracy. However, this last criterial is not essential, because the two principal parameters studied were if fibers foamed or not and the average diameter of both solid and hollow samples.

Hence, all samples on Figure 10 fulfilled the first condition showing no beads. Mostly all fibers accomplished the second criteria, besides singular exceptions. The low polymer concentration solution showed irregular larger fibers, specifically in the samples produced by 5 and 7.5 wt.% solutions (Figures 10a, 10b, 10c, 10d). In those samples there were higher chances of inducing defects, because the small fibers are more sensitive to perturbations, due to the low superficial tension or the size-scales implied. Those singular fibers which presented this defect was not be considered in the distribution of the diameters. For the last requirement, the average fiber diameter, the distribution standard deviation and the electrospun conditions of each sample were calculated (the data is registered in Table 1). The samples whose standard normalized deviation was close to 10%, which could be categorized as homogeneous, were 10 wt.% 20 cm (Figure 10f) and 15 wt.% (Figures 10i, 10j). The others had a minor degree of homogeneity, with wider distributions, until the samples like both 5 wt.% or 10 wt.% 15 cm (Figures 10a, 10b, 10e). Specifically, the sample 7.5 wt.% 20 cm (Figure 10d) consisted on a double distribution of the diameters, it was indicated in Table 1 (the lower value was represented in the graphs for simplicity).
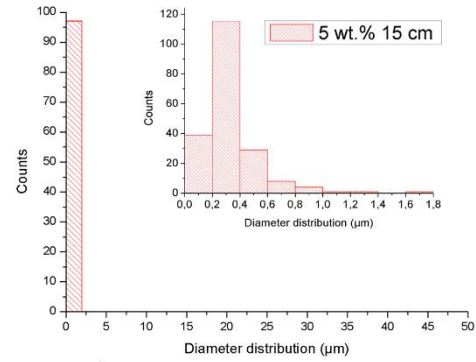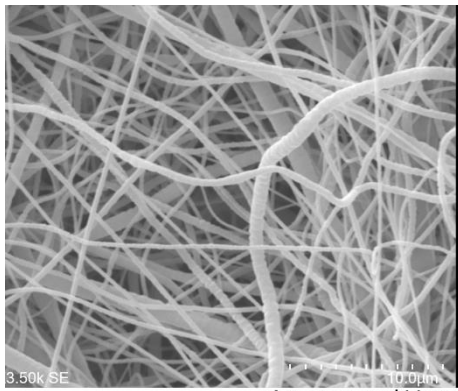
a) 5 wt.% 18 kV 15 cm 0.2 mL/h 45 %RH
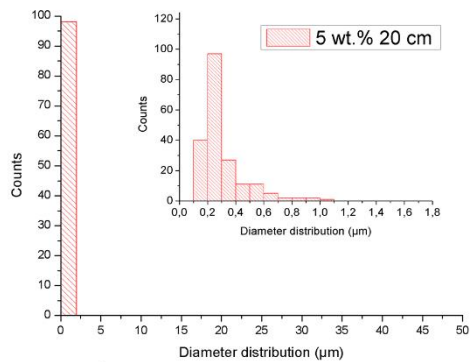
b) 5 wt.% 20 kV 20 cm 0.15 mL/h 42 %RH
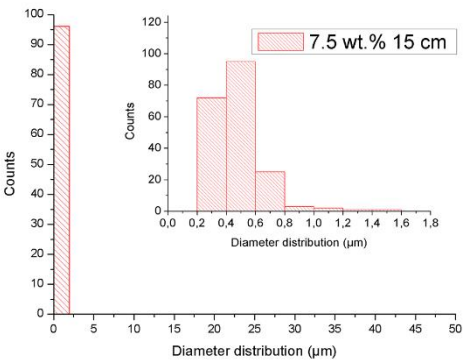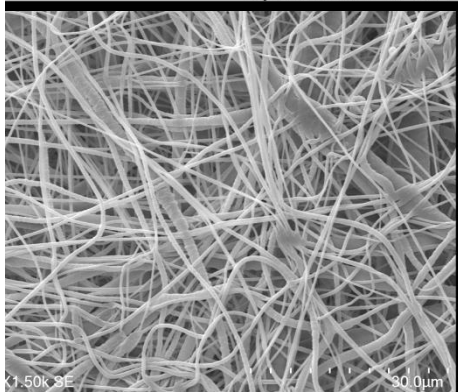
c) 7.5 wt.% 20 kV 15 cm 0.3 mL/h 33 %RH

d) 7.5 wt.% 20 kV 20 cm 0.6 mL/h 30 %RH

e) 10 wt.% 15 kV 15 cm 0.4 mL/h 33 %RH

f) 10 wt.% 20 kV 20 cm 0.7 mL/h 30 %RH

g) 15 wt.% 20 kV 15 cm 0.7 mL/h 37 %RH

h) 15 wt.% 20 kV 20 cm 1 mL/h 30 %RH

i) 17.5 wt.% 20 kV 15 cm 1 mL/h 30 %RH
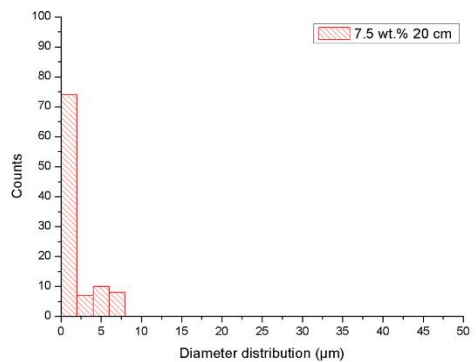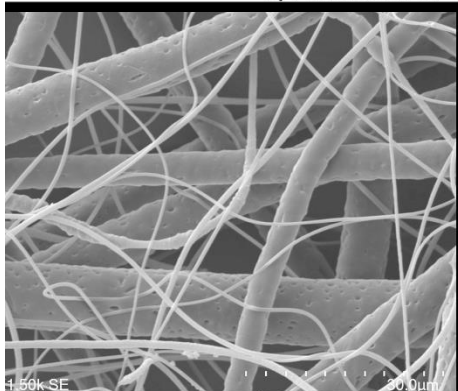
j) 17.5 wt.% 20 kV 20 cm 1 mL/h 30 %RH
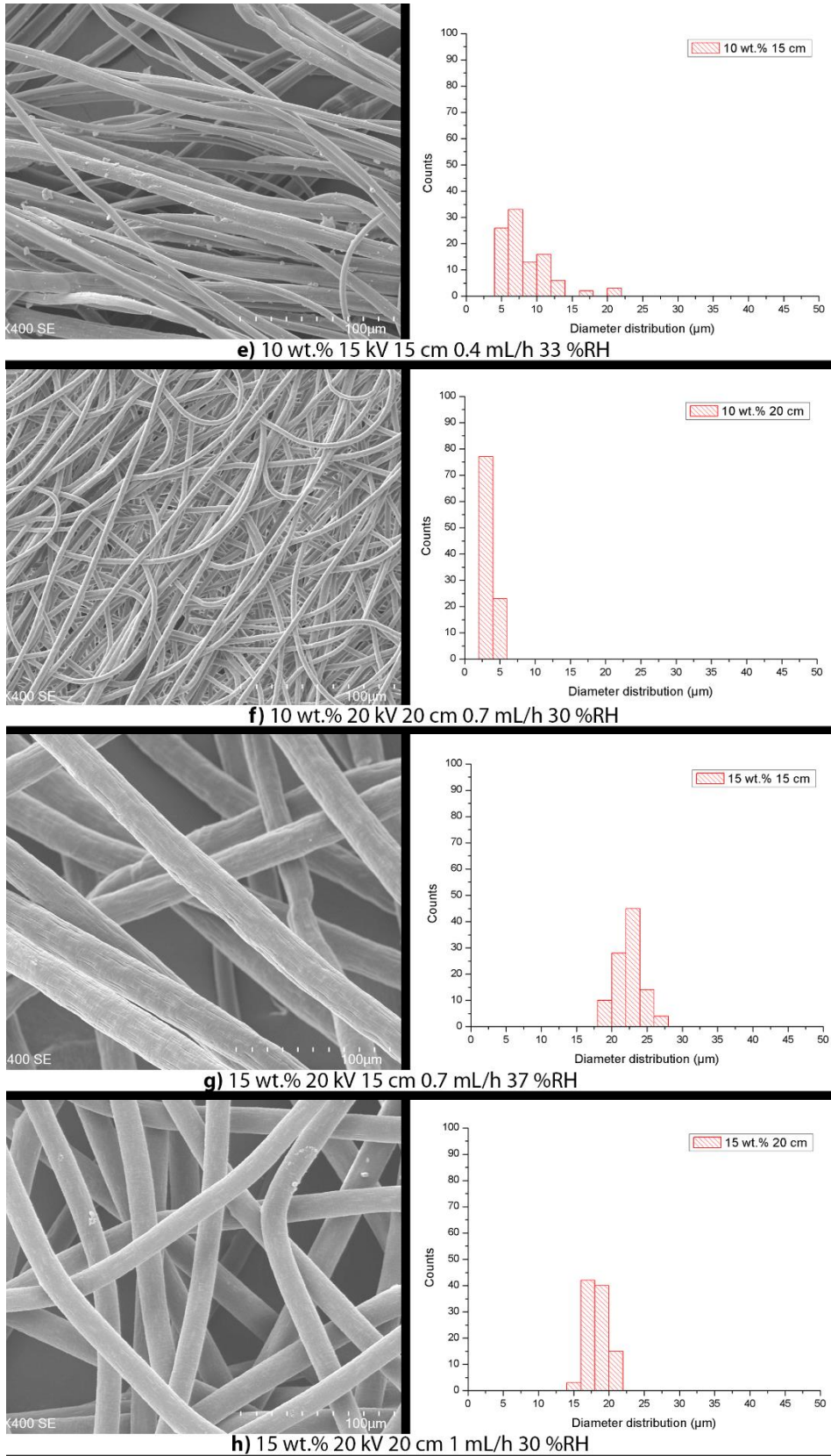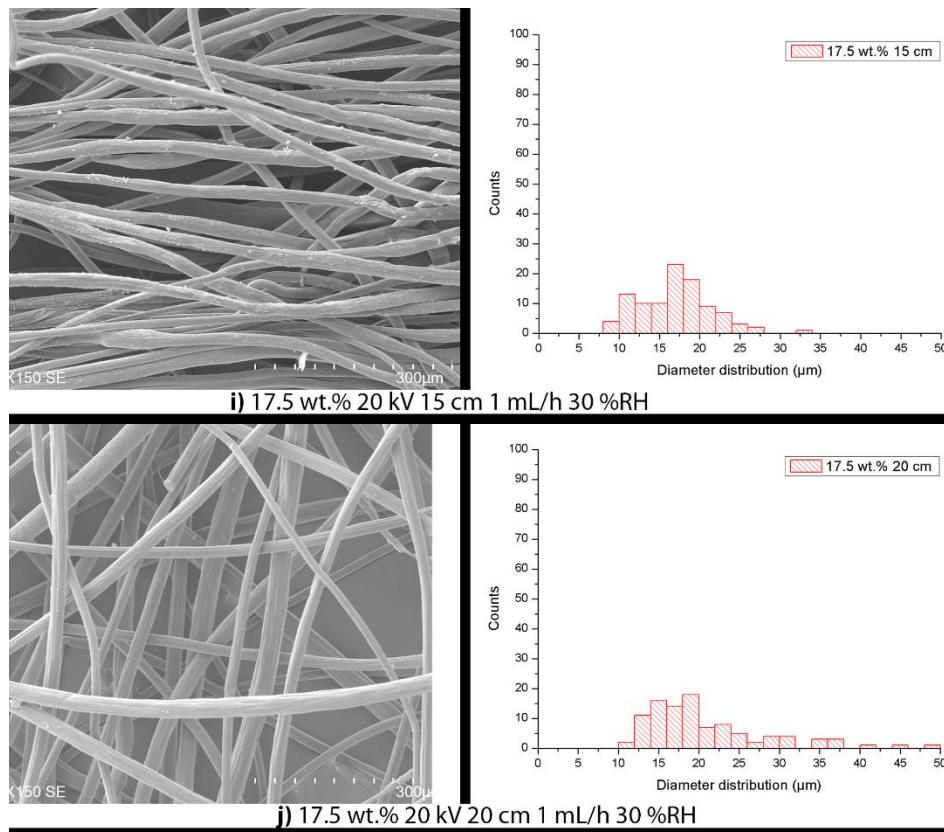
Figure 10 – SEM images of electrospun solid fibers. They are fabricated using different electrospun parameters and solution with different polymer concentration. The distance and the polymer concentrations are used to differentiate the samples, and the other parameters used are the indicated in the Table 1 and in the pictures. a) 5 wt.% and 15 cm, b) 5 wt.% and 20 cm, c) 7.5 wt.% and 15 cm, d) 7.5 wt.% and 20 cm, e) 10 wt.% and 15 cm, f) 10 wt.% and 20 cm, g) 15 wt.% and 15 cm, h) 15 wt.% and 20 cm, i) 17.5 wt.% and 15 cm, j) 17.5 wt.% and 20 cm. A diameter change has been observed while varying the polymer concentration, resumed in Figure 11.

*Table 1 – Data collection of the samples selected as optimized fibers, including the average diameter, the standard deviation, the relative standard deviation and the electrospun conditions (the needle-collector voltage, the flow rate, and the humidity). *The doble distribution of the fibers was found in 7.5 wt.% 20 cm.*

Polymer Concentration (wt.%)	Distance needle-collector (cm)	Average Diameter (µm)	Deviation (µm)	Relative Deviation	Electrospun Conditions
5	15	0.38	0.16	42%	18 kV 0. 2 mLh⁻¹ 45 %RH
	20	0.31	0.13	43%	20 kV 0. 15mLh⁻¹ 45 %RH
7.5	15	0.46	0.13	25%	20 kV 0. 3mLh⁻¹ 33 %RH
	20	1.0 – 5.2*	0.25 – 2.2*	25 - 41%*	20 kV 0. 6mLh⁻¹ 30 %RH
10	15	8.6	4.09	47%	15 kV 0. 4mLh⁻¹ 33 %RH
	20	3.6	0.45	12%	20 kV 0. 7mLh⁻¹ 30 %RH
15	15	22.4	1.9	8%	20 kV 0. 7mLh⁻¹ 37 %RH
	20	18.4	1.4	7%	20 kV 1 mLh⁻¹ 30 %RH
17.5	15	17.06	4.5	26%	20 kV 1 mLh⁻¹ 30 %RH
	20	19.62	6.0	30%	20 kV 1 mLh⁻¹ 30 %RH

After adjusting the electrospun parameters in favor of the production of homogeneous fibers, it has been demonstrated a dependence between the average diameter of the fibers and the polymer concentration used in the electrospun process (indicated in Figure 11), which occurs due to the viscosity increase[7]. When the viscosity is low, it facilitates thinner fibers, due to the low superficial tension and the low cohesion between the polymeric molecules[5]. However, if the tension surface overcomes viscosity, beads are originated. In the same way, if the polymer concentration is high enough it induces the chain entanglement between close polymeric molecules, originating higher-diameter fibers[5]. This dependence have been reported by other authors like Al-Qadhi et al.[8] using polysulfone (PSF), who obtained three different fiber structures based on: "beads, beads-on-strings and free-beads fibers", being the low polymer concentrations assigned to bead-structures. Other polymers like chitosan are used to produce the electrospun fibers as well, and the same relationship have been observed[18]. Consequently, higher polymer concentration implies higher diameter fibers. Even so, the solid samples obtained were the same as Enis et al.[47] had obtained. They carried out close to the same electrospun process with PCL, but with a slight variation in some parameters (solvent used chloroform: ethanol 9:1 proportion, concentration 14-16-18-20%, flow rate 0.4mL-1mL/h, voltage 12-15kV, distance 20cm). The double distributions, the presence of beads in low polymer concentration and the high standard deviation were observed in the micro and nano ranged fibers production.
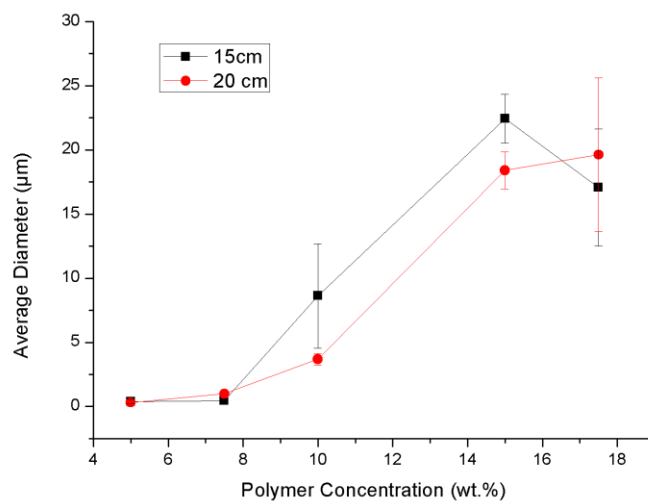
Figure 11 – Relationship between average diameter of fibers and polymer concentration is represented. In the graph 7.5 wt.% 20 cm consist on a double distribution but only 1μm fibers are indicated.

3.3. Foamed Fibers

The samples of both solid and foamed fibers are represented in Figure 12, a superficial image and an cross section one were represented on all cases, with the aim of observing the superficial morphology and how the solid fiber have evolved into a hollow one respectively. However, the nanofibers presented more difficulties in the fracture process, so the cross-section pictures, where single fibers could be appreciated, were not possible in some cases (Figures 12a, 12b and 12d). There are samples of solid fibers used in the gas dissolution foaming process (Figure 12 and letters without apostrophes), and the product samples after removing the PVOH film (Figure

12 and letters with apostrophes), i.e., the hollow ones. The hollow fibers were named by their base electrospun conditions for this work purposes. In cases where 5 or 7.5 wt.% fibers were used, corresponding with a mix of nano and early micro diameter scales, the thinner ones did not seem to foam while the large ones did (Figures 12a', 12b' 12c'). The low diameter fibers probably remained intact because the gas escaped too fast from its inside, avoiding the nucleation points to form. Upon the micro-size diameter, the hollow fibers were produced, this demonstrated a potential minimum value to allow fibers foaming under the conditions used in this work. In the double distribution sample (7.5 wt.% 20 cm (Figure 12d')) occurred the same effect that the mentioned before, where the thinner fibers were not foamed and around 5 µm fibers shown up as hollow fibers. All other samples (10 wt.% (Figures 12e' and 12f'), 15 wt.% (Figures 12g' and 12h') and 17.5 wt.% (Figure 12j' and 12i')) were become hollow fibers. After the foaming, the fibers of 7.5 wt.% 20 cm and 10 wt.% 20 cm (Figures 12d and 12f) shown superficial porosity with the diameters about 1 µm, and the hollow inner cores with the diameters of 7.6 and 4.0 µm, respectively. Whereas the other samples, with higher diameter (10 wt.% 15 cm, 15 wt.% and 17.5 wt.%), presented a solid external surface without any pores. The fibers with the solid surface maintained the same morphology than the solid initial samples, e.g., the longitudinal scratches in the solid fibers of 17.5 wt.% could be appreciated also in the obtained hollow fibers (Figures 12i and 12j). The thickness of the edges was proportional to the size of the fibers, being about a few hundred of nanometers on smaller fibers (Figures 12a and 12b) and reaching up to a few micrometers in the thicker one (Figures 12k and 12l). In case of the sample produced at 15 wt.% 20 cm, the PVOH was not completely removed and the fibers were covered and connected by a layer. It was clearly shown in its image of the cross section (Figure 12i') where the fiber ends and the PVOH starts. Probably a defect occurred in the removing process, for example, staying out of the water bath in one of the 15 minute washing cycles. Furthermore, the measure of the average diameter counted with higher difficulties, due to it was not possible to always to measure accurately.

Barroso-Solares et al.[36] were the first to publish combining these two techniques (the electrospinning and the gas dissolution foaming), obtaining hollow fibers with the diameters close to 10 µm. The two different foaming possibilities were explored, on the one hand, they reported porous hollow microfibers by using the one-step foaming. On the other hand, while using two-step foaming, i.e., using the RT for the saturation time, and heating the sample after depressurization, a solid skin in the hollow fibers are produced. In this work all samples were fabricated by using the one-step process, so according to the bibliography, the superficial porosity can be expected, but, on the contrary, the solid skin fibers are produced for higher diameters. Actually, the samples 7.5 wt.% 20 cm (Figure 12d) and 10 wt.% 20 cm (Figure 12f) showed the superficial porosity, yet the thicker fibers did not have the porosity despite being produced by a one-step procedure (except defects). As the production route of the solid fibers was slightly different in the previous work, the further work should be performed on this field to fully understand the mechanisms involved in the formation of the hollow fibers and the surface porosity.

a)   5 wt.% 18 kV 15 cm 0.2 mL/h 45 %RH   a')

b)   5 wt.% 20 kV 20 cm 0.15 mL/h 45 %RH   b')

c)   7.5 wt.% 20 kV 15 cm 0.3 mL/h 33 %RH   c')

d)   7.5 wt.% 20 kV 20 cm 0.6 mL/h 30 %RH   d')

e) 10 wt.% 15 kV 15 cm 0.4 mL/h 33 %RH e')

f) 10 wt.% 20 kV 20 cm 0.7 mL/h 30 %RH f')

g) 15 wt.% 20 kV 15 cm 0.7 mL/h 37 %RH g')

h) 15 wt.% 20 kV 20 cm 1 mL/h 30 %RH h')
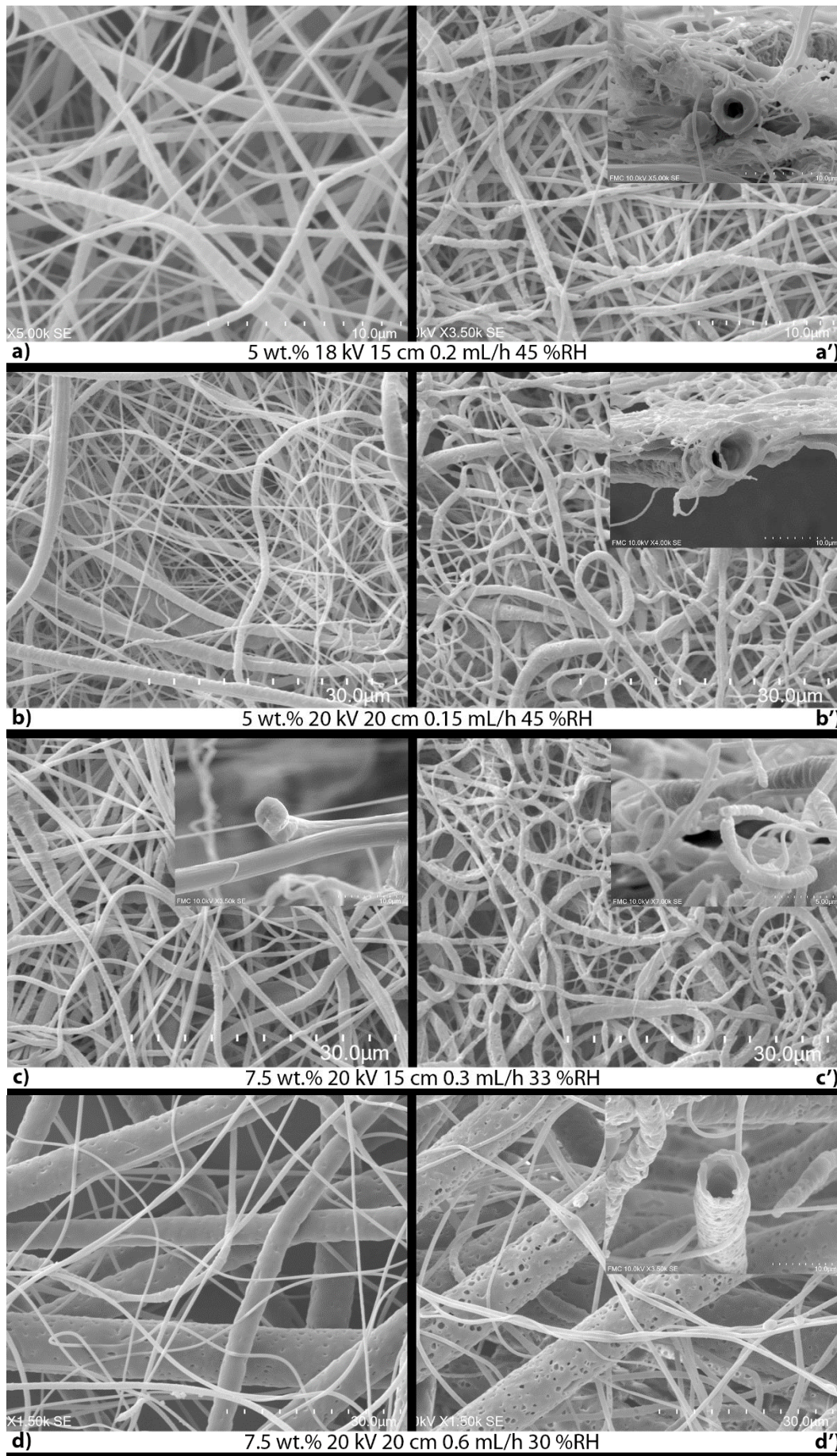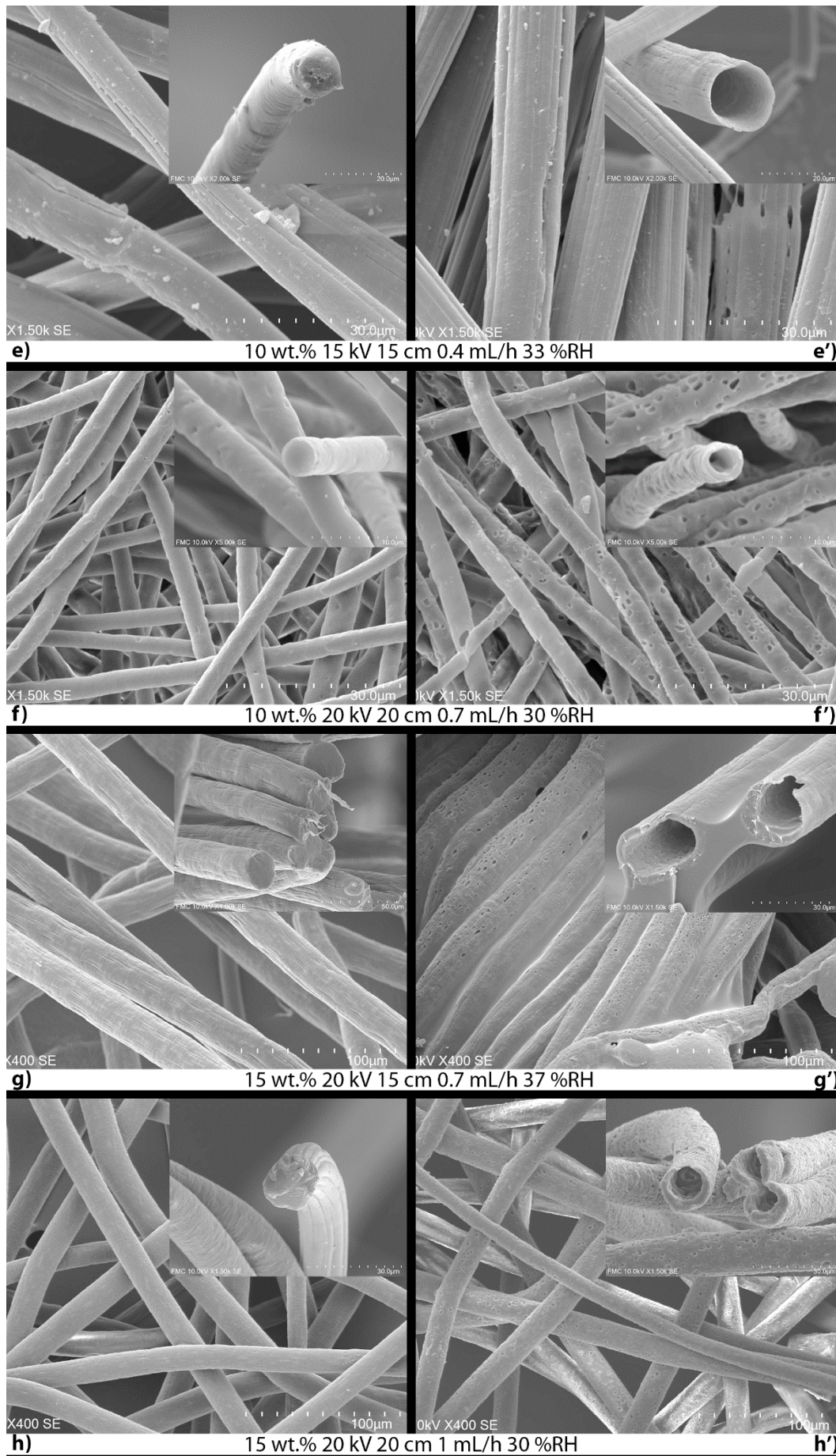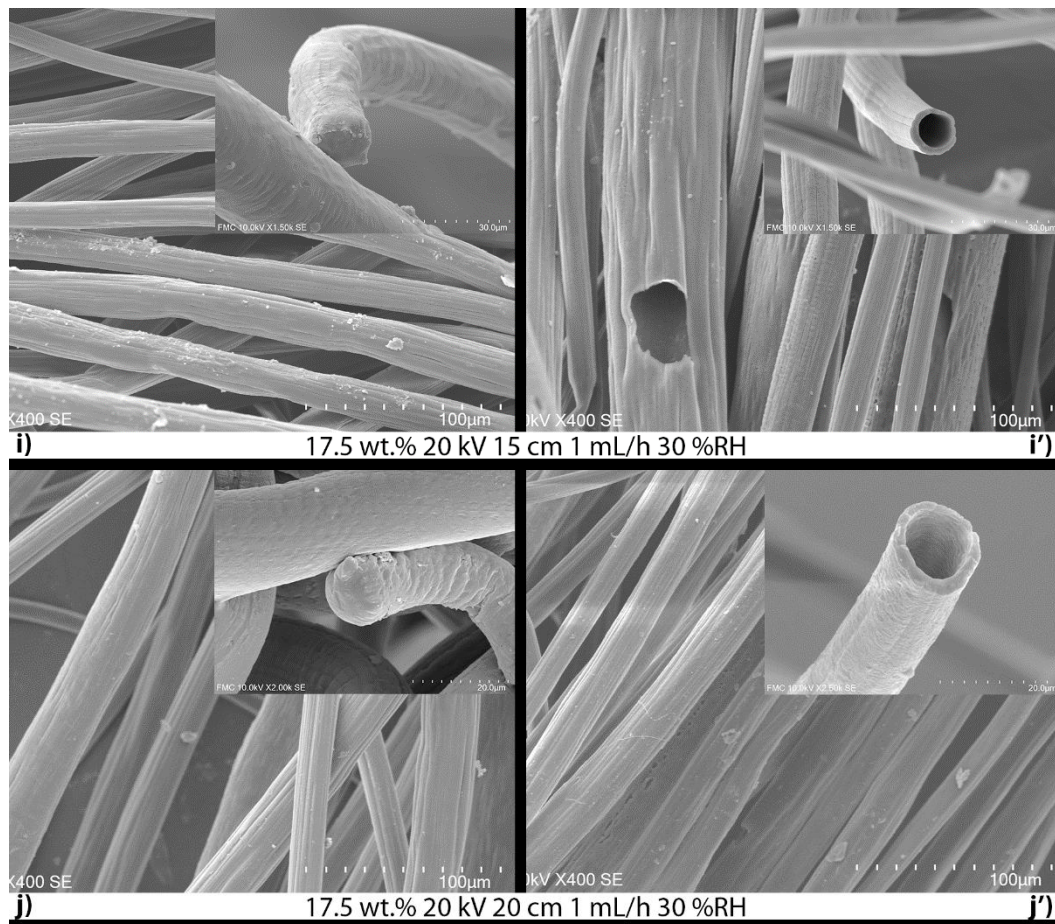
Figure 12 – SEM images of electrospun solid and hollow fibers. Letters indicate solid fibers and letters with aphostrophs represent hollowed fibers. They are fabricated using samples of the different electrospun conditions and the same gas dissolution foaming dissolution path. The samples are differentiated by electrospun parameters those are produced. Those are: a) 5 wt.% and 15 cm, b) 5 wt.% and 20 cm, c) 7.5 wt.% and 15 cm, d) 7.5 wt.% and 20 cm, e) 10 wt.% and 15 cm, f) 10 wt.% and 20 cm, g) 15 wt.% and 15 cm, h) 15 wt.% and 20 cm, i) 17.5 wt.% and 15 cm, j) 17.5 wt.% and 20 cm. All samples are foamed using the same conditions (45 °C temperature and 30 MPa pressure).

Not all micro-sized fibers were completely hollowed, some of them were composed of small pores, indicated in Figure 13. Some fibers foamed with small pores inside (Figure 13c), while other consists on larger pores (Figure 13a) and the other samples even stayed as solid fibers (Figure 13b). Furthermore, some fibers showed superficial defects, as big pores, or breakages (as showed in Figure 12i')). Moreover, in this work some samples not included in above tables presented defects in form of spherules (Figure 14). This effect is produced because the imbibing process had imperfections, and not all fibers were completely covered, inducing that when the temperature was rise above the melting temperature, the polymer could melt and create deformations. And, after the PVOH removement, as-like-beads structures can be found in the samples.

a) 17.5 wt.% 20 kV 20 cm 1mL/h 30 %RH | **b)** 10 wt.% 20 kV 20 cm 0.7 mL/h 30 %RH

c) 10 wt.% 15 kV 15 cm 0.4 mL/h 35 %RH
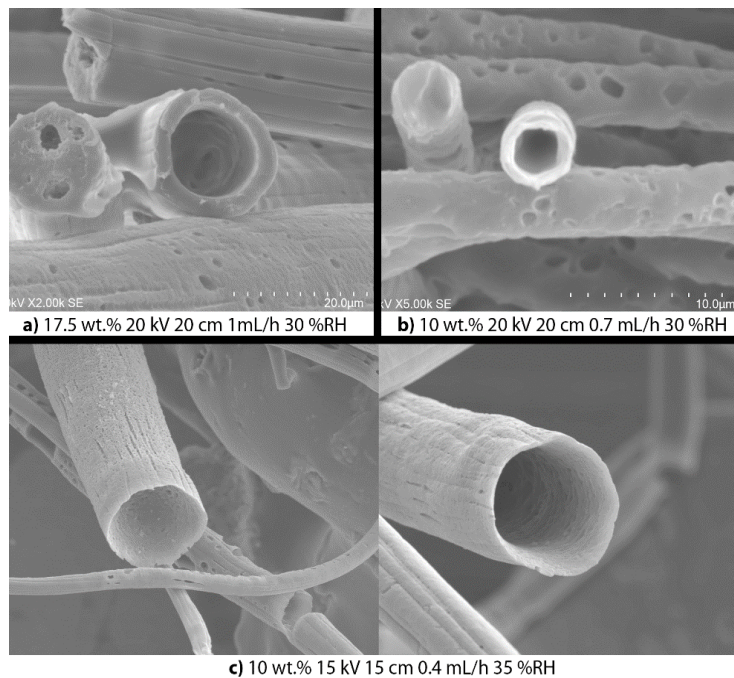
Figure 13 – Representation of hollow fiber and solid fiber of a) 17.5 wt.% 20 kV 20 cm 1 mL/h 30 %RH b) 10 wt.% 20 kV 20 cm 0.7 mL/h 30 %RH and c) 10 wt.% 15 kV 15 cm 0.4 mL/h 35 %RH, by SEM images. It is shown how not all fibers in the samples have foamed.

a) 17.5 wt.% 20 kV 15 cm 0.8 mL/h 35 %RH | **b)** 15 wt.% 20 kV 20 cm 0.8 mL/h 30 %RH
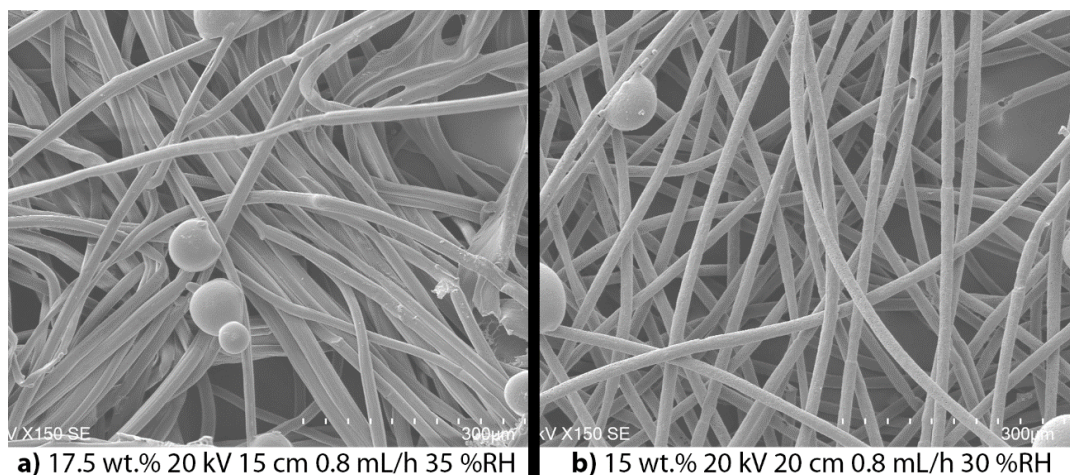
Figure 14 – Representation of hollow fiber and solid fiber of a)17.5 wt.% 20 kV 15 cm 0.8 mL/h 35 %RH and b) 15 wt.% 20 kV 20 cm 0.8mL/h 30 %RH, by SEM images. Spherules appeared in samples with higher average diameter.

The results obtained from 7.5 wt.% 20 cm sample were useful to understand qualitatively how the gas dissolution foaming process interact with the nanometer and low micrometer range fibers. Comparing the diameter distribution from before and after foaming (Figures 15a and 15b), thinner distribution remained as solid fibers, but small notches appeared in fibers between 500 – 1000 nm (Figure 15c). Next, the high-diameter distribution suffered a displacement from 5.2 to 7.6 μm, corresponding with the hollow fibers observed in the cross section of Figure 12d'.

a)

b)

c) 7.5 wt.% 20 kV 20 cm 0.6 mL/h 30 %RH
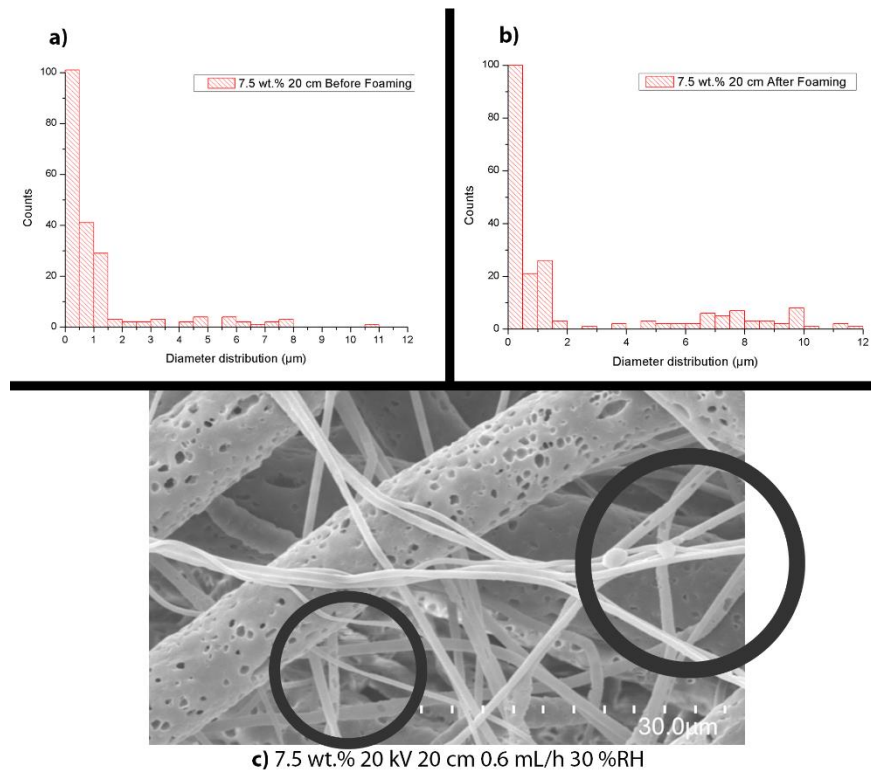
Figure 15 – Comparison between diameter distribution is represented in a and b, consisting of 7.5 wt.% 20 cm before and after foaming, respectively. In c, in the same sample, notches can be observed in smaller fibers.

Finally, to study consequences of the foaming process in the diameter of fibers, the expansion foaming ratio has been calculated for all samples (represented in Figure 16), i.e., the relationship between the post and pre foaming diameters. Furthermore, the comparison between the post and pre foaming diameters are indicated in Figure 17a and 17b, corresponding with the samples of 15 cm and 20 cm, respectively. The average expansion ratio of the foamed fibers is generally above the unity, but close to it in some cases, showing a diameter increase of between 10-30% in most cases.
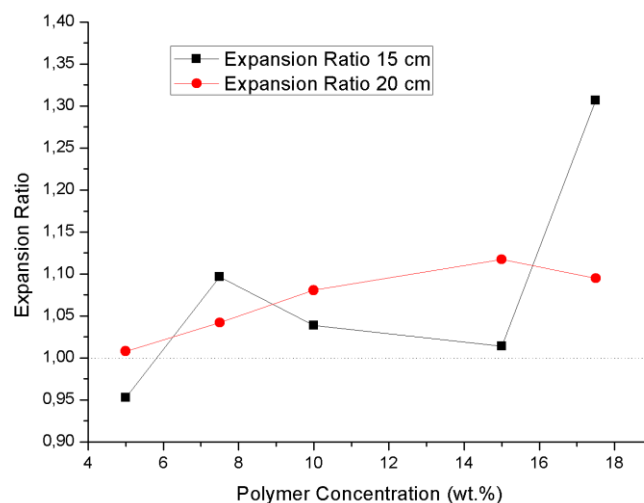
Figure 16 – Expansion ratio of fibers, i.e., relation between diameter of hollow and solid fibers.
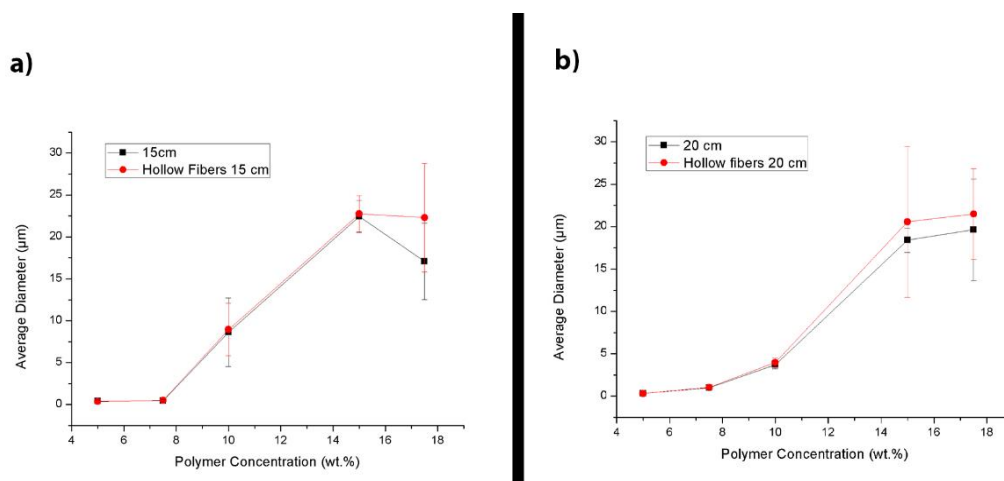
Figure 17 – The relationship between diameter of the fibers and the polymer concentration in a and b, the samples of 15 and 20 cm, respectively. The hollow and solid fibers are represented in each case.

In the case of fibers with irregularities, such as the outliers that appear in the 5 wt.% and 7.5 wt.% samples, they were not taken in account because it is impossible to follow how the foaming process was carried out. The expansion ratio of the 5 wt.% 15 cm samples was lower than the unity (specifically, 0.95), however, it was not produced by a real decrease in the diameters of the fibers. This value is due to the most part of the fibers have not foamed and the statistical errors implied. With the aim of a deeper analysis of the cases where it is not clear if the fibers have foamed (5 wt.% and 7.5 wt.%), the different histograms have been represented. First, the 5 wt.% diameter distributions (Figures 18a and 18b) allowed to confirm that no expansion has occurred. It was assumed that the size of the fibers was not enough to allow the nucleation points to form or create the pores at the foaming conditions employed. Next, in the analysis of the 7.5 wt.% 15 cm sample, it was possible to appreciate an expansion in the diameters after the foaming process. However, it was not possible to affirm that those fibers were hollowed, as not-interconnected pores can origin the expand instead. From this result, it seems that a minimum diameter is necessary to the fibers to expand at the foaming conditions employed, making that smaller fibers remain apparently intact after the gas dissolution foaming path. The minimum fiber diameter determined in this work as able to foam (foaming PCL fibers at 30 MPa and 45 °C) was around 500 nm. This is a significant result, as this is the first time that polymeric fibers with diameters below the micron have been foamed (i.e., only foamed micrometric fibers were obtained in the previous work).

27
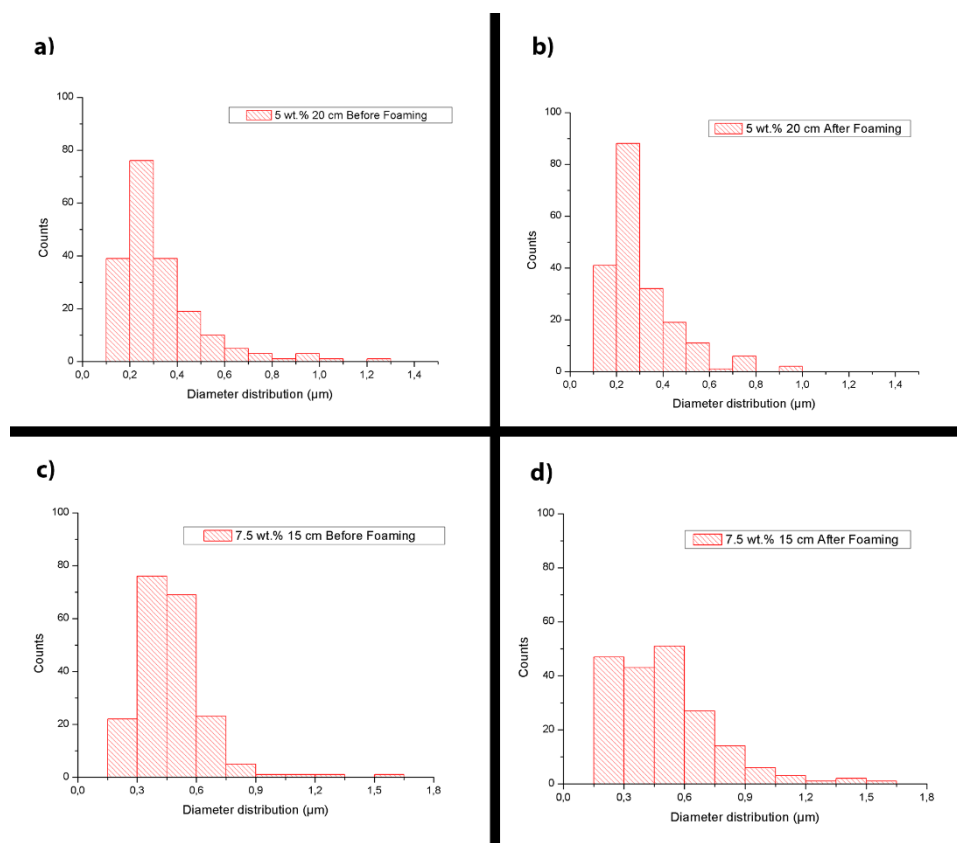
Figure 18 – The diameter distribution of 5 wt.% 20 cm (a, b) and 7.5 wt.% 15 cm (c, d) before and after suffering the gas dissolution process. Histograms a and b showed the same distribution, while in the case of c and d a small expansion in distribution in fibers have been observed.

However, the main precedent of this work[36] found a clear increase of the average fiber diameter from 6.5 μm to around 11 μm, so a clear difference is set at this point, the expansion ratio is clearly higher (about 70%) than the obtained in this work (up to 30%). Moreover, in the work carried out by Barroso-Solares et al.[36] the size of the external walls of the fibers reported for micro-size fibers were around a hundred nanometers, while we are reporting walls with wide of micrometers. In Figure 19 this effect can be appreciated, while in this work, thicker-wall samples formed lower-diameter hollow fibers, but the other fibers with higher diameter presented a thinner wall.

Accordingly, it seems that the wall thickness could be directly related to the reached expansion ratio (i.e., higher diametral expansions induce a higher stretching of the polymer around the hollow structure, leading to thinner polymer walls). In addition, further work is required to address the differences found in the expansion ratio between both works, in which slight differences exist in the production of the initial solid PCL fibers. As a first approach to understand the foaming behavior of the fibers, this work attempted to study more in detail their properties by Differential Scanning Calorimetry.

10 wt.% 20 kV 20 cm 0.7 mL/h 30 %RH
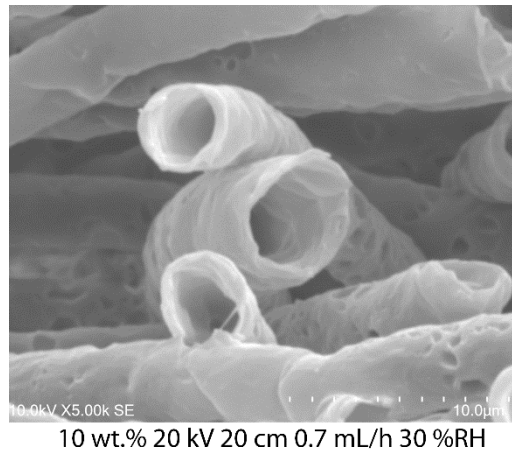
Figure 19 – Different fiber size and different wall thickness is observed in the samples with higher homogeneity.

3.4. Differential Scanning Calorimetry (DSC)

Crystallinity and melting temperature of both electrospun solid and foamed hollow fibers are indicated in Table 2, and their relationship with the electrospun fiber polymer concentration or the diameter size in Figure 17. The melting temperature of all the samples was about 60 °C, as expected for PCL, without finding significant differences between the different fibers or due to the foaming process. On the contrary, the crystallinity values obtained showed a broader dispersion from 60 to 80%. It is well-known that the rise of the crystallinity of a polymer is a limiting factor for its foaming by gas dissolution foaming. However, no clear trends can be identified from the available data, but the evolution of the crystallinity of the thinner fibers (5 wt.%), which were unable to foam, from 63 to 80% due to the foaming process, suggests that this approach could be suitable to improve our understanding about these materials. Accordingly, further future work on this direction should be performed.
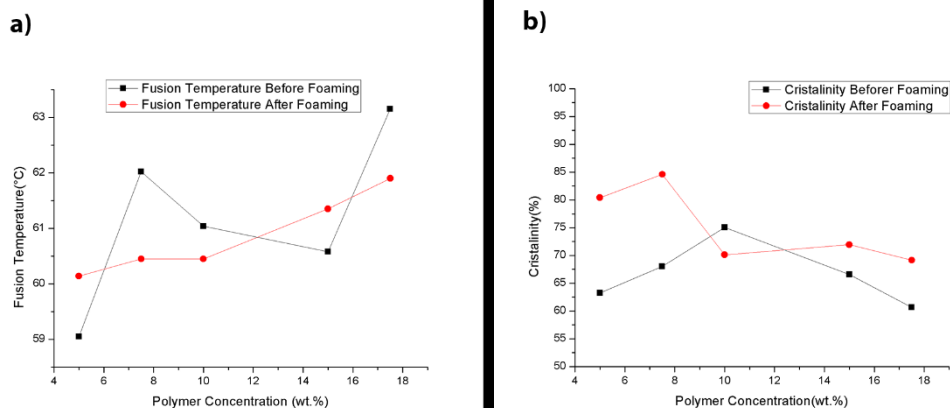
Figure 20 – The relation between the fusion temperature and the crystallinity are represented for each polymer concentration sample. No dependence has been reported in this work between the crystallinity and the electrospun conditions.

29

Table 2 – The data collection of DSC results. The fusion temperature and the crystallinity.

Polymer Concentration (wt.%)	Fusion temperature (°C)		Crystallinity (%)	
	Before Foaming	After Foaming	Before Foaming	After Foaming
5	59.05	60.14	63.25	80.40
7.5	62.02	60.45	68.01	84.59
10	61.04	60.45	75.07	70.13
15	60.58	61.35	66.59	71.95
17.5	63.15	61.9	60.66	69.15

4. Conclusions

PCL solid electrospun fibers have been produced, allowing to analyze the influence of the main parameters in the process. The different polymer concentrations were used to generate various sizes of fibers, from a few hundreds of nanometers to around 20 μm. The flow rate was firstly determined for each polymer concentration. After that, the increase of voltage resulted in a decrease of the diameters of the fibers. Then, the flow rate effect was more complex, because the two different described in its correspondent epigraph. Moreover, the humidity was inducing a wider and bimodal distribution of diameters and the changing morphology of the thicker fibers. This research has established a minimum diameter to the fibers to foam from a gas dissolution foaming route, as other authors previously did with nano and micro particles. The use of PVOH, a well-known CO_2 easy-removable barrier, as a cover for the fibers allowed the foaming of the small sizes. Furthermore, the hollow fibers of low micro-size scale were produced using an eco-friendly and easy-scalable path and a biocompatible and biodegradable polymer, being of a great interest in biomedical applications. The different surface morphologies were produced depending on the size of the fibers, obtaining pores in smaller ones and a thicker solid skin in higher-diameter fibers. However, the largest source of the numerical error in this work is related with the statists. The electrospun technique allow the generation of nano and microfibers but they are not completely homogeneous. Furthermore, the process of taking the SEM images is destructive with the samples, as first they need to be covered with a layer of gold, this makes that the part of the sample initially studied with the SEM images cannot be foamed and its specific evolution after the gas dissolution cannot be studied. These limitations cause that for a more accurate knowledge in this subject, it exists the need of repeating the whole process several times. Besides the statistical errors, further investigation is needed in the gas dissolution foaming parameters, such as the pressure and the temperature saturation. In addition, the two-step gas dissolution foaming could allow interesting results related to the superficial morphology and skin appearance of fibers.

Finally, in this work different state-of-the-art techniques of polymer characterization were applied to understand and measure the different properties and features, allowing to connect the knowledge acquired in the master's degree with the real applications. As an example, the optic microscopy, which has been used in the laboratory practical courses, has been intensively used in this work. Moreover, the gas dissolution foaming process has been used in nanomaterials. The different properties of polymers took place in this work, such as the crystallinity, the glass transition temperature, and the melting temperature of polymers. The electrospun process has been used to produce the samples, which induce the familiarization with the technique, and learning how the different parameters affect in the

result. The equipment utilized on this work by the student is addressed in Annex I, and all images from electrospun samples are in Annex II. Furthermore, the student has been familiarized with the dynamics of organization in a real investigation group, and learnt how the cooperation between laboratory technicians, investigators and other students allows the projects to be successfully completed, until the final development of a scientific article.

5. Bibliography

1.   Munj, H. R. & Tomasko, D. L. Polycaprolactone-polymethyl methacrylate electrospun blends for biomedical applications. *Polym. Sci. - Ser. A* **59**, 695–707 (2017).

2.   Cheng, M., Qin, Z., Hu, S., Yu, H. & Zhu, M. Use of electrospinning to directly fabricate three-dimensional nanofiber stacks of cellulose acetate under high relative humidity condition. *Cellulose* **24**, 219–229 (2017).

3.   Zaarour, B., Zhu, L. & Jin, X. Controlling the surface structure, mechanical properties, crystallinity, and piezoelectric properties of electrospun PVDF nanofibers by maneuvering molecular weight. *Soft Mater.* **17**, 181–189 (2019).

4.   Nezarati, R. M., Eifert, M. B. & Cosgriff-Hernandez, E. Effects of humidity and solution viscosity on electrospun fiber morphology. *Tissue Eng. - Part C Methods* **19**, 810–819 (2013).

5.   Liu, Y. *et al.* A Review on Recent Advances in Application of Electrospun Nanofiber Materials as Biosensors. *Curr. Opin. Biomed. Eng.* (2020) doi:10.1016/j.cobme.2020.02.001.

6.   Kulkarni, A., Bambole, V. A. & Mahanwar, P. A. Electrospinning of Polymers, Their Modeling and Applications. *Polym. - Plast. Technol. Eng.* **49**, 427–441 (2010).

7.   Tan, X. M. & Rodrigue, D. A review on porous polymeric membrane preparation. Part II: Production techniques with polyethylene, polydimethylsiloxane, polypropylene, polyimide, and polytetrafluoroethylene. *Polymers (Basel).* **11**, (2019).

8.   Al-Qadhi, M. *et al.* Preparation of superhydrophobic and self-cleaning polysulfone non-wovens by electrospinning: influence of process parameters on morphology and hydrophobicity. *J. Polym. Res.* **22**, (2015).

9.   Rahmati Nejad, M., Yousefzadeh, M. & Solouk, A. Electrospun PET/PCL small diameter nanofibrous conduit for biomedical application. *Mater. Sci. Eng. C* **110**, 110692 (2020).

10.   Barroso-Solares, S. *et al.* Oil removal from water-oil emulsions using magnetic nanocomposite fibrous mats. *RSC Adv.* **6**, 71100–71107 (2016).

11.   Zhao, J., Sun, Z., Shao, Z. & Xu, L. Effect of surface-active agent on morphology and properties of electrospun PVA nanofibres. *Fibers Polym.* **17**, 896–901 (2016).

12.   Wang, Z. *et al.* Controllable deposition distance of aligned pattern via dual-nozzle near-field electrospinning. *AIP Adv.* **7**, 1–10 (2017).

13.   Eleyas, A., Bakar, S., Halif, N. & Yahud, S. 2017 the Effect of Flow Rate , Concentration , and Voltage on Diameter of. **2**, 71–78 (2017).

14.   Bakar, S. S. S., Fong, K. C., Eleyas, A. & Nazeri, M. F. M. Effect of Voltage and Flow Rate

Electrospinning Parameters on Polyacrylonitrile Electrospun Fibers. *IOP Conf. Ser. Mater. Sci. Eng.* **318**, (2018).

15. Duan, G. & Greiner, A. Air-Blowing-Assisted Coaxial Electrospinning toward High Productivity of Core/Sheath and Hollow Fibers. *Macromol. Mater. Eng.* **304**, 2–6 (2019).

16. Veerabhadraiah, A. *et al.* Development of polyvinyl acetate thin films by electrospinning for sensor applications. *Appl. Nanosci.* **7**, 355–363 (2017).

17. Yongyi, Y. *et al.* Polysulfone nanofibers prepared by electrospinning and gas / jet-electrospinning. 334–339 (2006) doi:10.1007/s11458-006-00.

18. Jaruayporn, Kobsak, R. Effect of parameters on the morphology and fibre diameters of edible electrospun chitosan-cellulose acetate-gelatin hybrid nanofibres. **03038**, 4 (2018).

19. Kuchi, C., Harish, G. S. & Reddy, P. S. Effect of polymer concentration, needle diameter and annealing temperature on TiO2-PVP composite nanofibers synthesized by electrospinning technique. *Ceram. Int.* **44**, 5266–5272 (2018).

20. Yu, D. G. *et al.* Electrospinning of concentrated polymer solutions. *Macromolecules* **43**, 10743–10746 (2010).

21. Razzaz, Z., Mohebbi, A. & Rodrigue, D. Effect of processing conditions on the cellular morphology of polyethylene hollow fiber foams for membrane applications. *Cell. Polym.* **37**, 169–188 (2018).

22. Ramakrishnan, R. *et al.* Effect of Humidity on Formation of Electrospun Polycaprolactone Nanofiber Embedded with Curcumin using Neeaddleless Electrospinning. *Mater. Today Proc.* **19**, 1241–1246 (2019).

23. Huang, L., Bui, N. N., Manickam, S. S. & McCutcheon, J. R. Controlling electrospun nanofiber morphology and mechanical properties using humidity. *J. Polym. Sci. Part B Polym. Phys.* **49**, 1734–1744 (2011).

24. Agarwal, S., Greiner, A. & Wendorff, J. H. Functional materials by electrospinning of polymers. *Prog. Polym. Sci.* **38**, 963–991 (2013).

25. Barroso-Solares, S., Pinto, J., Nanni, G., Fragouli, D. & Athanassiou, A. Enhanced oil removal from water in oil stable emulsions using electrospun nanocomposite fiber mats. *RSC Adv.* **8**, 7641–7650 (2018).

26. Vu, D. L., Li, Y. Y., Lin, T. H. & Wu, M. C. Fabrication and humidity sensing property of UV/ozone treated PANI/PMMA electrospun fibers. *J. Taiwan Inst. Chem. Eng.* **99**, 250–257 (2019).

27. Yanilmaz, M. Evaluation of electrospun PVA/SiO2 nanofiber separator membranes for lithium-ion batteries. *J. Text. Inst.* **111**, 447–452 (2020).

28. Alavarse, A. C. *et al.* Tetracycline hydrochloride-loaded electrospun nanofibers mats based on PVA and chitosan for wound dressing. *Mater. Sci. Eng. C* **77**, 271–281 (2017).

29. Wang, B., Zheng, H., Chang, M. W., Ahmad, Z. & Li, J. S. Hollow polycaprolactone composite fibers for controlled magnetic responsive antifungal drug release. *Colloids Surfaces B Biointerfaces* **145**, 757–767 (2016).

30. Yuriar-Arredondo, K. *et al.* Nanofiber-based Matrimid organogel membranes for battery separator. *J. Memb. Sci.* **546**, 158–164 (2018).

31.   Wahyudiono *et al.* Formation of PVP hollow fibers by electrospinning in one-step process at sub and supercritical CO2. *Chem. Eng. Process. Process Intensif.* **77**, 1–6 (2014).

32.   Skvortsov, I. Y. *et al.* Fibers spinning from poly(trimethylsilylpropyne) solutions. *J. Appl. Polym. Sci.* **137**, 1–10 (2020).

33.   Nazely Diban, Suvi Haimi, Lydia Bolhuis-Versteeg, Sandra Teixeira, Susanna Miettinen, André Poot, Dirk Grijpma, D. S. Development and characterization of poly(ε-caprolactone) hollow fiber membranes for vascular tissue engineering. 29–37 (2013) doi:https://doi.org/10.1016/j.memsci.2013.03.024.

34.   Cheung, T. W. & Li, L. A review of hollow fibers in application-based learning: from textiles to medical. *Text. Res. J.* **89**, 237–253 (2019).

35.   Demeuse, M. T. *Production and applications of hollow fibers*. *Handbook of Textile Fibre Structure* vol. 2 (Woodhead Publishing Limited, 2009).

36.   Suset Barroso-Solares, Daniel Cuadra-Rodriguez, Maria Luz Rodriguez-Mendez, Miguel Angel Rodriguez-Perez, and J. P. A new generation of hollow polymeric microfibers produced by gas dissolution foaming. (2020) doi:10.1039/C9TB02641J.

37.   Pinto, J., Dumon, M., Pedros, M., Reglero, J. & Rodriguez-Perez, M. A. Nanocellular CO2 foaming of PMMA assisted by block copolymer nanostructuration. *Chem. Eng. J.* **243**, 428–435 (2014).

38.   Pinto, J. *et al.* Solid skin characterization of PMMA/MAM foams fabricated by gas dissolution foaming over a range of pressures. *Defect Diffus. Forum* **326**–**328**, 434–439 (2012).

39.   Martín-de León, J., Bernardo, V. & Rodríguez-Pérez, M. ángel. Low density nanocellular polymers based on PMMA produced by gas dissolution foaming: Fabrication and cellular structure characterization. *Polymers (Basel).* **8**, (2016).

40.   Notario, B. *et al.* Experimental validation of the Knudsen effect in nanocellular polymeric foams. *Polymer (Guildf).* **56**, 57–67 (2015).

41.   Martín-de León, J., Bernardo, V. & Rodríguez-Pérez, M. Á. Key Production Parameters to Obtain Transparent Nanocellular PMMA. *Macromol. Mater. Eng.* **302**, 3–7 (2017).

42.   Orsi, S., Di Maio, E., Iannace, S. & Netti, P. A. Hollow micro- and nano-particles by gas foaming. *Nano Res.* **7**, 1018–1026 (2014).

43.   Vroman, I. & Tighzert, L. Biodegradable polymers. *Materials (Basel).* **2**, 307–344 (2009).

44.   Abràmoff, M. D., Magalhães, P. J. & Ram, S. J. Image processing with imageJ. *Biophotonics Int.* **11**, 36–41 (2004).

45.   Rueden, C. T. *et al.* ImageJ2: ImageJ for the next generation of scientific image data. *BMC Bioinformatics* **18**, 1–26 (2017).

46.   Yuan, X. Y., Zhang, Y. Y., Dong, C. & Sheng, J. Morphology of ultrafine polysulfone fibers prepared by electrospinning. *Polym. Int.* **53**, 1704–1710 (2004).

47.   Enis, I. Y., Vojtech, J. & Sadikoglu, T. G. Alternative solvent systems for polycaprolactone nanowebs via electrospinning. *J. Ind. Text.* **47**, 57–70 (2017).

Annex I

1. Electrospinning Set Up
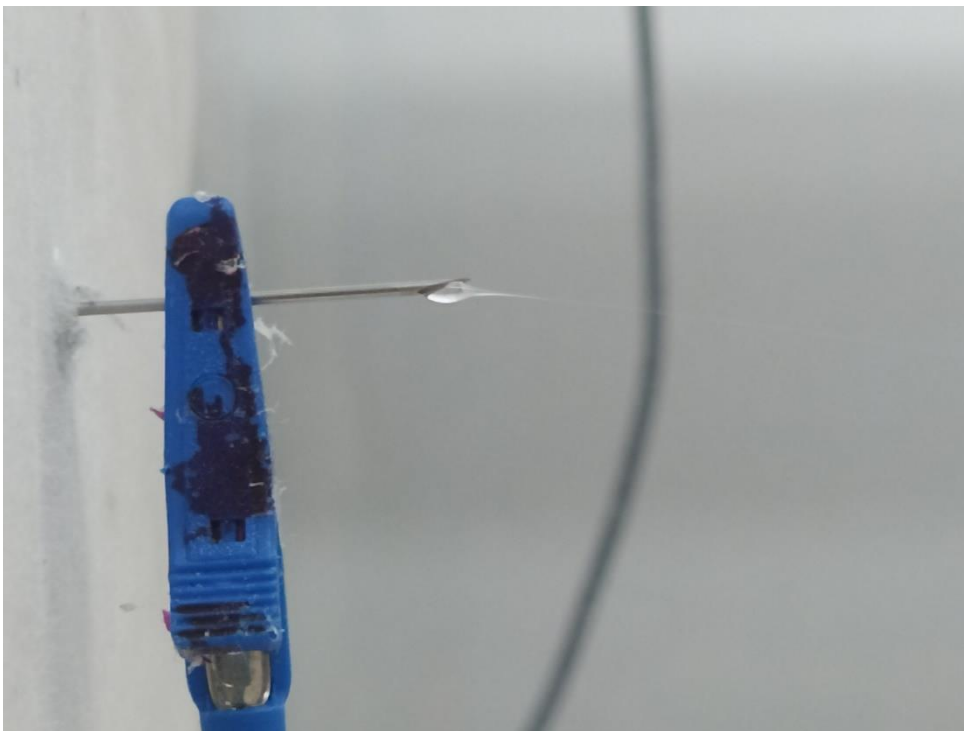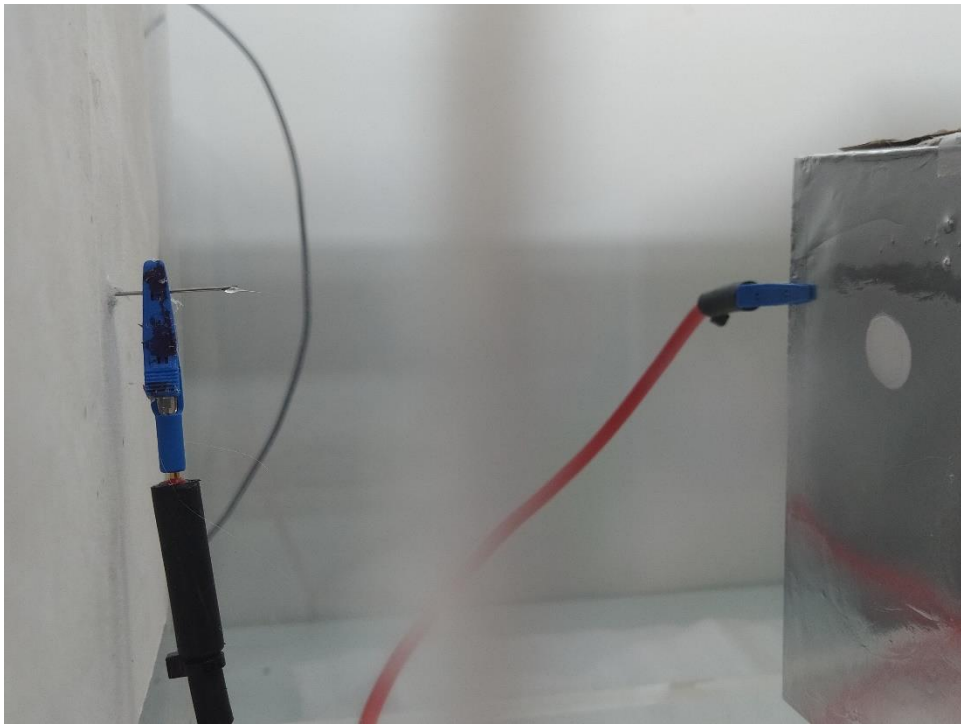
2. Optic Microscope
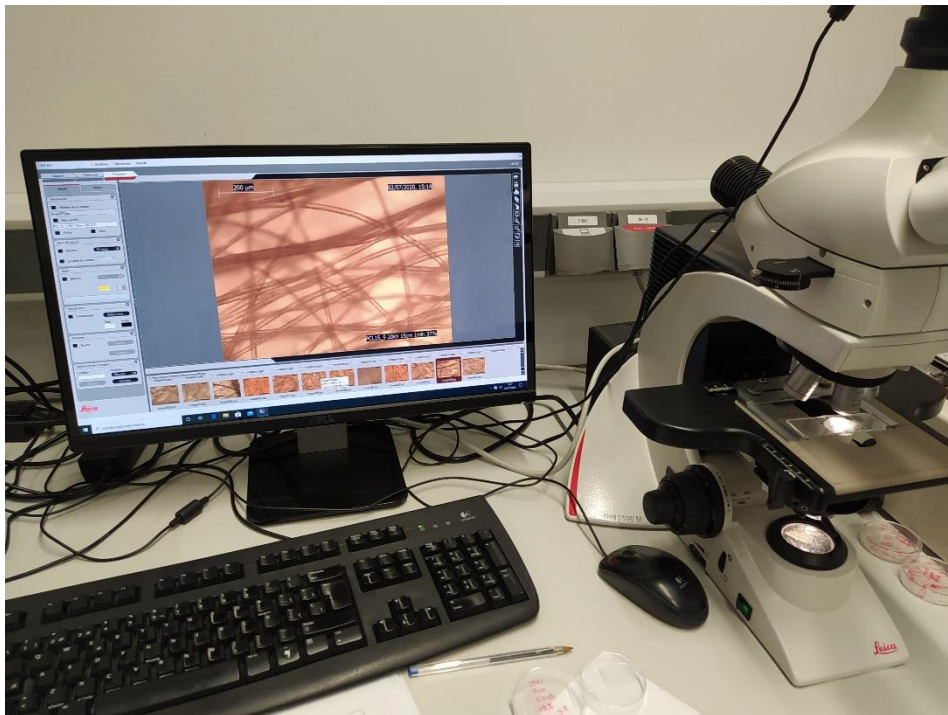
3. Gas Foaming Set Up
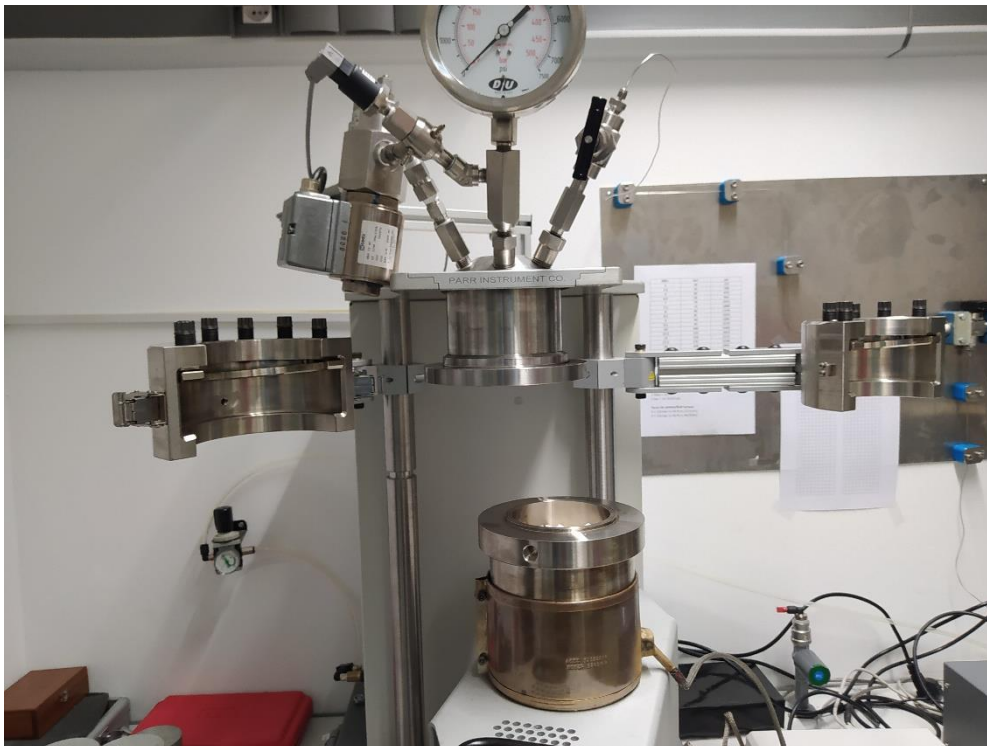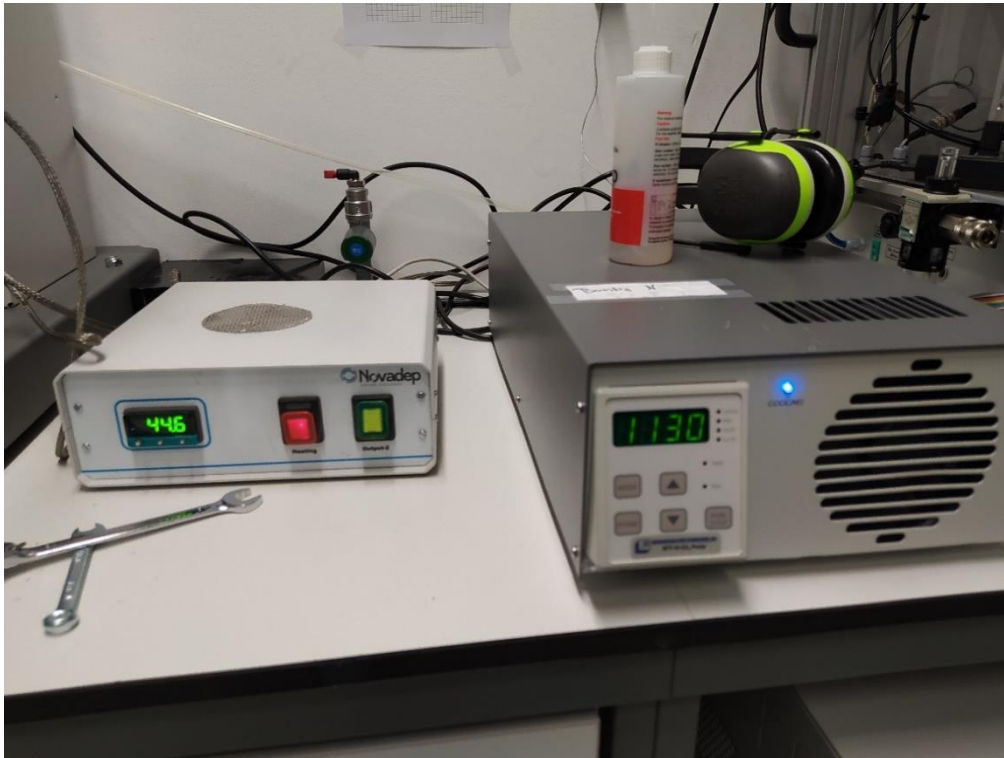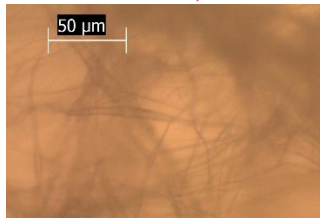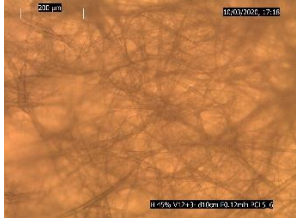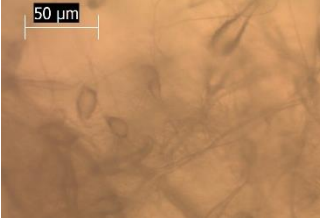
4. Ultrasonic Water Bath
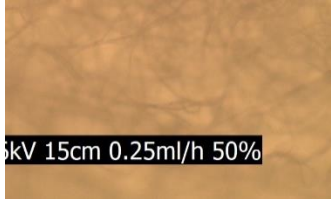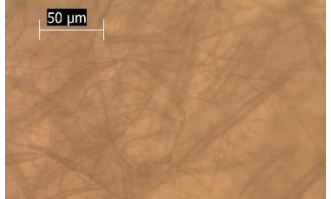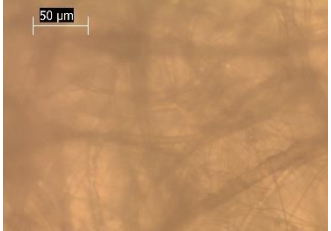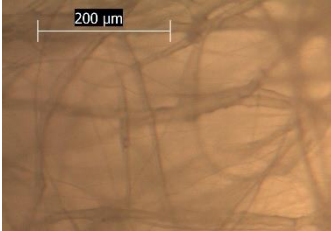
Annex II
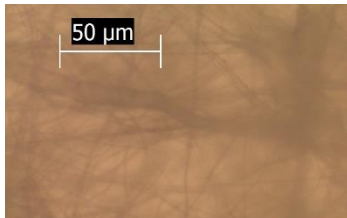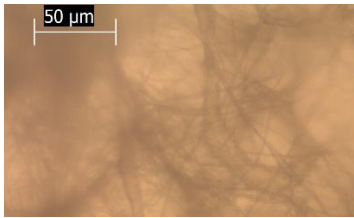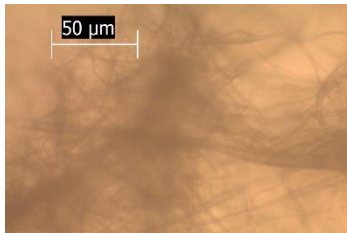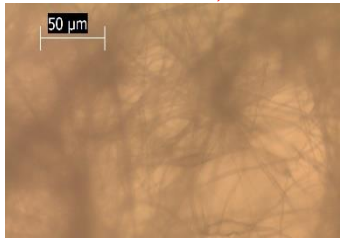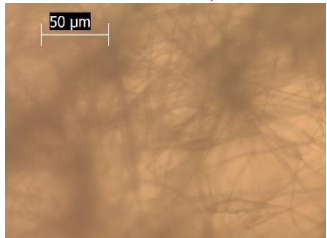
In the next pages is shown the compilation of all samples produced and analyzed in this work. To classify them a color code has been stablished, representing the degree of homogeneity and the presence of beads. The red color indicates completely inhomogeneous samples and/or with beads, the orange is for samples which show a higher homogeneity, and the green is for the most homogeneous samples produced in that polymer concentration without beads. The distance is varied in the columns, the voltage in the rows, and the name of each sample is organized like: "Polymer concentration (wt.%)"."The number of the sample" – "The flow rate used (mL/h)", H "the humidity used (%RH)".

5 wt.%
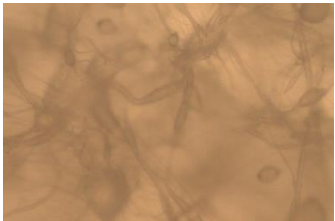
Voltage (KV)	Distance (cm)			
	10	15	17	20
14		5.5-0.2 mL/h, H 45%		
15	5.6-0.12 mL/h, H 45%	5.30- 0.3mlh 42%		

16	5.8-0.25 mL/h, H 27%	5.12-0.2 mL /h, H 36%		
17		5.10-0.2 mL /h, H 37%		
18				5.3-0.2 mL /h, H 44%
20		5.11-0.2 mL /h, H 37%	5.16-0.3 mL /h, H 34%	5.1-0.4 mL /h, H 44%
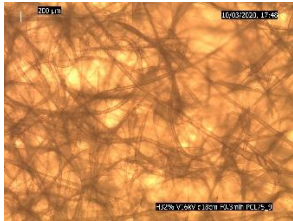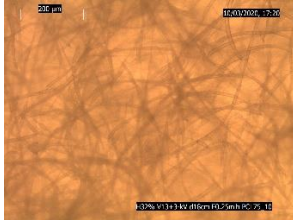
		5.14-0.7 mL /h, H 42%		5.2-0.2 mL /h, H 44%
		5.15-0.3 mL /h, H 37%		5.4-0.2 mL /h, H 45%
		5.19-0.3 mL /h, H 37%		5.17-0.3 mL /h, H 35%
		5.27-0.3mlh 44%		5.20-0.8 mL /h, H 30%
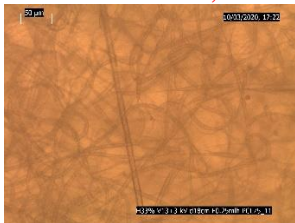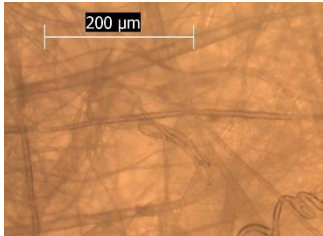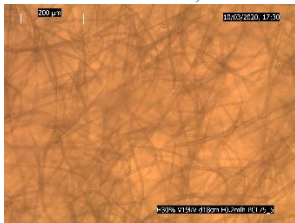
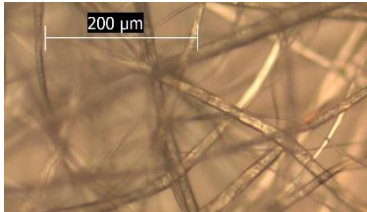|		5.28-0.2mlh 44%		5.27 – 0.3mL/h H 44%
		5.29-0.15mlh 44%		
21		5.22-0.3 mL /h, H 41%		5.21-0.8 mL /h, H 30%
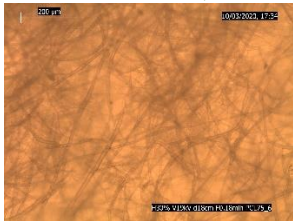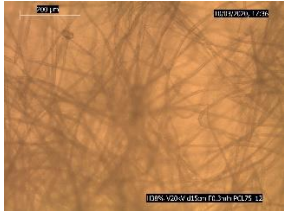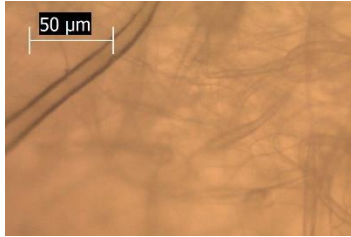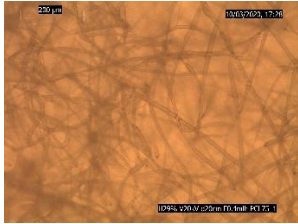
		5.23-0.4ml/h H 41%		
22		5.24-0.2ml/h H 50%		
25		5.25-0.3ml/h H50%		
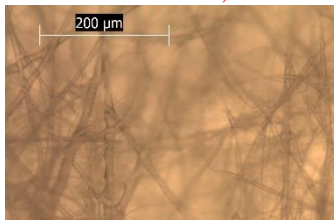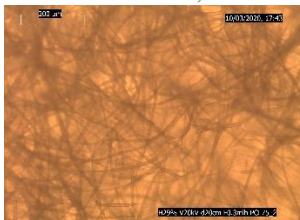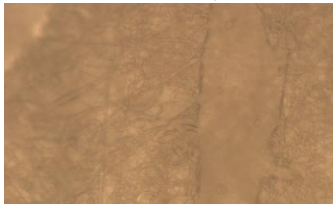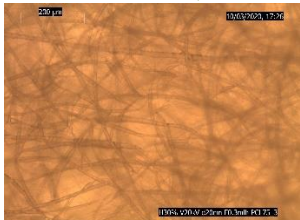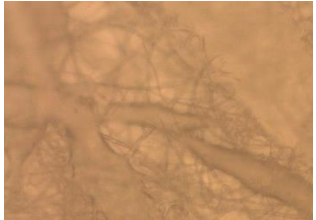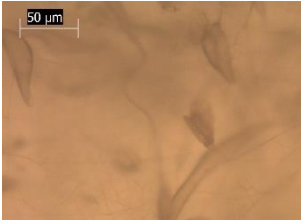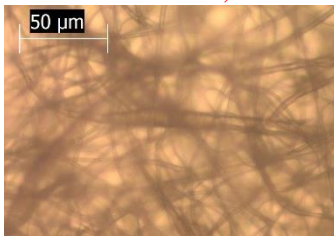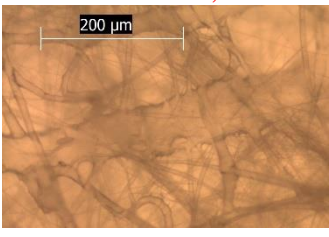
		5.26-0.5ml/h H50%		
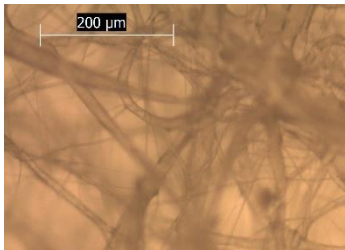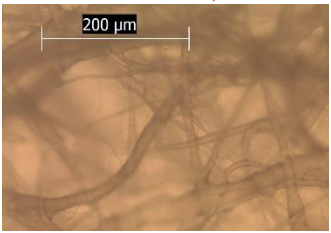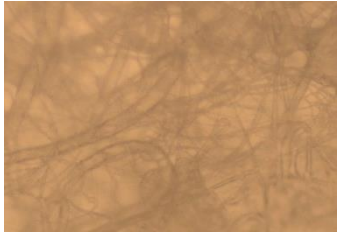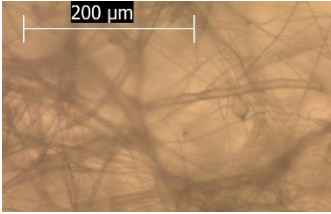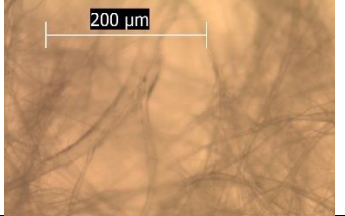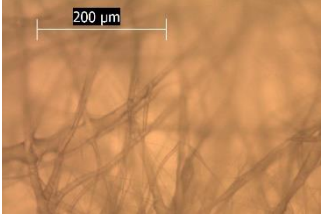
7.5 wt.%

Voltage (KV)	Distance (cm)				
	10	15	18	20	25
15		7.5.28 – 0.25mL/h, 33%			
16			7.5.9-0.3 mL/h, H 32%		
			7.5.10-0.25 mL/h, H 32%		
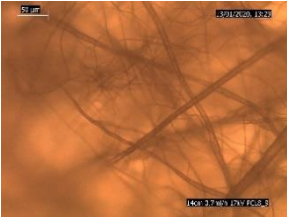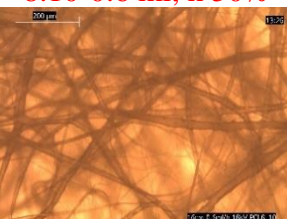
		7.5.11-0.25 mL/h, H 32%		
18	7.5.13-0.4 mL/h, H 37% 			
19		7.5.5-0.2 mL/h, H 29% 		
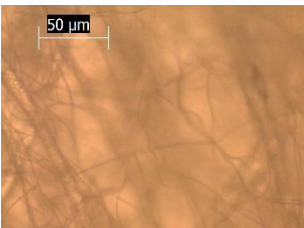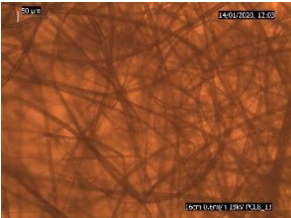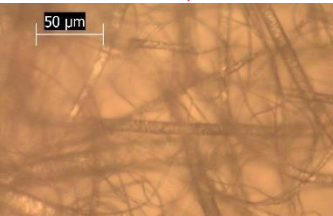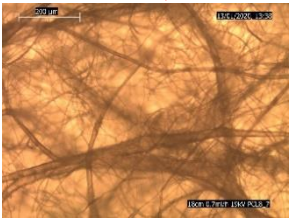
			7.5.6-0.18 mL/h, H 29%		
			7.5.7-0.14 mL/h, H 29%		
			7.5.8-0.16 mL/h, H 29%		
20		7.5.12-0.3 mL/h, H 37%	7.5.4-0.3 mL/h, H 29%	7.5.1-0.4 mL/h, H 28%	
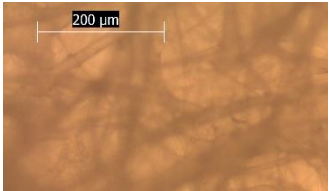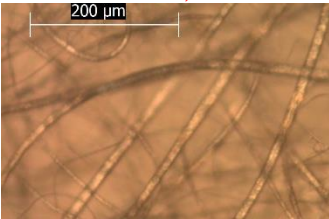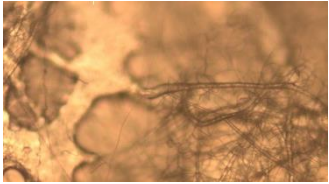
		7.5.18-0.5 mL/h, H 38%		7.5.2-0.3 mL/h, H 28%	
		7.5.20-0.5 mL/h, H 41%		7.5.3-0.2 mL/h, H 28%	
		7.5.21-0.4 mL/h, H 41%		7.5.14-0.8 mL/h, H 37%	
		7.5.22 – 0.3ml/h, H 41%		7.5.17-0.5 mL/h, H 38%	
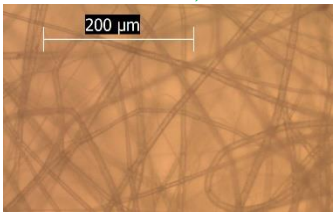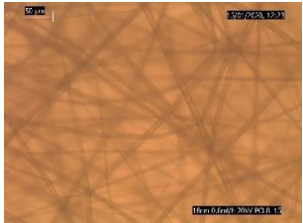
		7.5.23 – 0.5ml/h H 41%		7.5.19-0.8 mL/h, H 35%	
		7.5.25 – 0.3ml/h H 42%		7.5.29 – 0.6mL/h, H 29%	
		7.5.27 – 0.2mL/h, H 33%			
21				7.5.16-0.6 mL/h, H 38%	7.5.15-0.6 mL/h, h 37%

8 wt.%

Voltage (KV)	Distance (cm)			
	14	16	18	20
17	8.9-0.7 ml, h 50% 			
18		8.8-0.7 ml, h 50% 		
		8.10-0.6 ml, h 50% 		
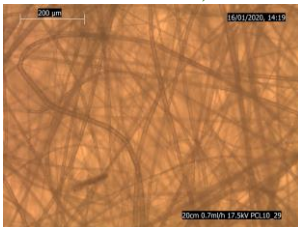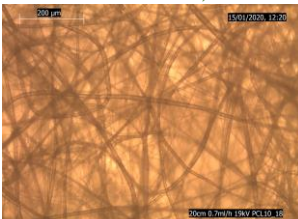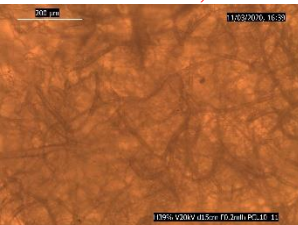
		8.11-0.7 ml, h 50% 	
		8.13-0.6 ml, h 29% 	
19		**8.4-0.8 ml, h 50%** 	
		8.7-0.8 ml, h 50% 	

20			8.1-0.8 ml, h 50%	
			8.2-0.8 ml, h 50%	
			8.5-0.7 ml, h 50%	
			8.6-07 ml, h 50%	
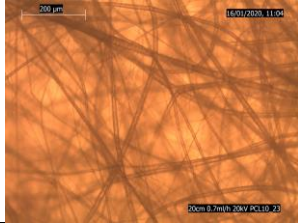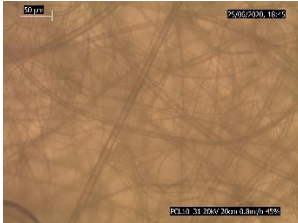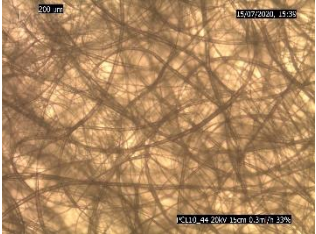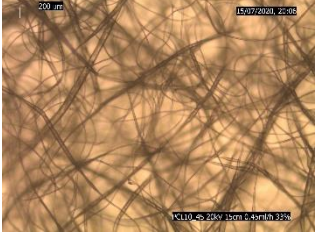
| | | | 8.14-0.6 ml, h 29% | |
| | | | 8.15-0.6 ml, h 29% | |
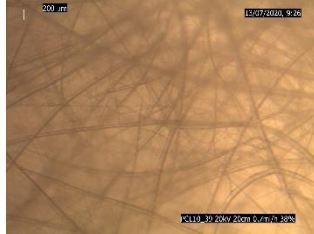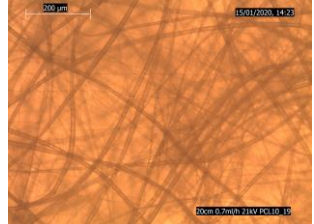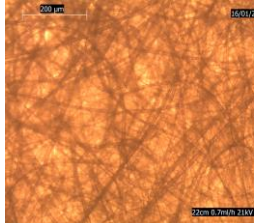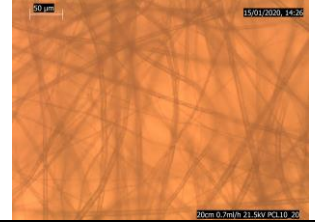
10 wt.%
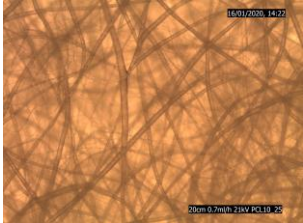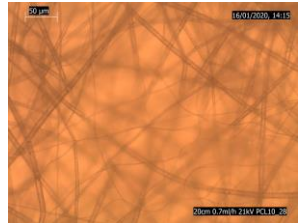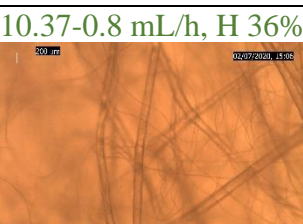
Voltaje (KV)	Distance (cm)				
	15	18	19	20	22
15	10.16-0.7 mL/h, H 33%				
	10.46-0.4mL/h, H 33%				
	10.47-0.3mL/h, H 33%				
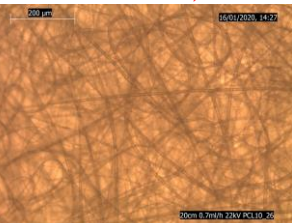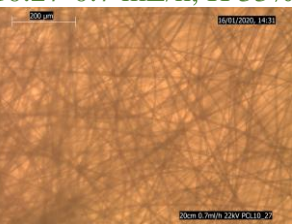
17	10.42-0.6 mL/h, H 50%			10.29-0.7 mL/h, H 35%	
19	10.9-0.6 mL/h, H 50%			10.18-0.7 mL/h, H 30%	
	10.11-0.5 mL/h, H 50%				
	10.12-0.6 mL/h, H 50%				

	10.13-0.7 mL/h, H 45%				
20	**10.3-1 mL/h, H 50%**	**10.2-1 mL/h, H 50%**	**10.21-0.7 mL/h, H 30%**	**10.1-1 ml/h, H 50%**	**10.22-0.7 mL/h, H 30%**
	10.38-0.7 mL/h, H 35%	**10.14-0.7 ml/h, H 29%**		**10.15-0.7 mL/h, H 30%**	
	10.40-0.9 mL/h, H 35%			**10.17-0.7 mL/h, H 30%**	
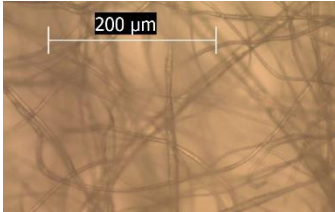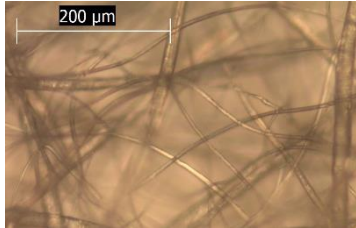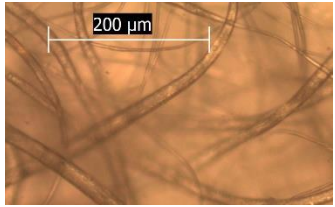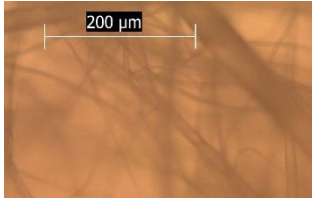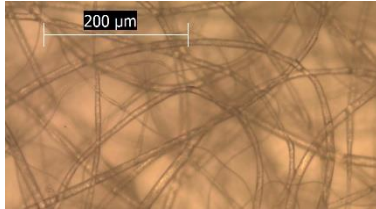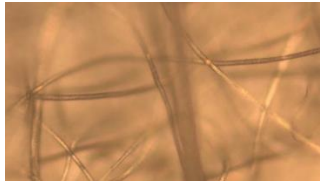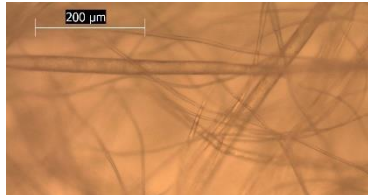
			10.23-0.7 mL/h, H 35%	
10.43-0.5mL/h, H33%			10.31-0.8 mL/h, H 45%	
10.44-0.3mL/h, H33%			10.32-0.7 mL/h, H 39%	
10.45-0.45mL/h, H33%			10.34-0.6 mL/h, H 27%	
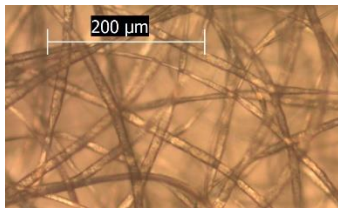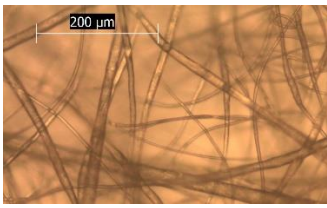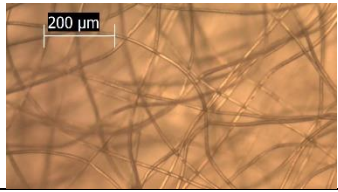
			10.39-0.7 mL/h, H 38%	
			10.42-0.7 mL/h, H 35%	
21	10.41-0.9 mL/h, H 35%		10.5-1 mL/h, H 50%	10.19-0.7 mL/h, H 30%	10.24-0.7 mL/h, H 35%
			10.6-0.7 mL/h, H 50%	10.20-0.7 mL/h, H 30%	

			10.25-0.7 mL/h, H 35%	
			10.28-0.7 mL/h, H 35%	
			10.35-0.8 mL/h, H 30%	
			10.37-0.8 mL/h, H 36%	
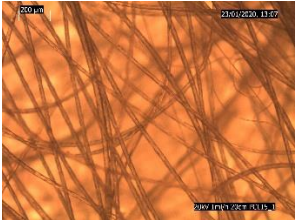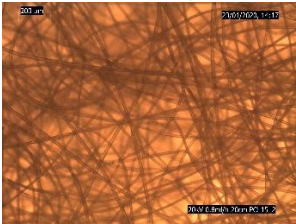
22	10.7-0.3 mL/h, H 50%			10.4-1 mL/h, H 50%	
				10.26-0.7 mL/h, H 33%	
				10.27-0.7 mL/h, H 33%	
				10.36-0.8 mL/h, H 33%	
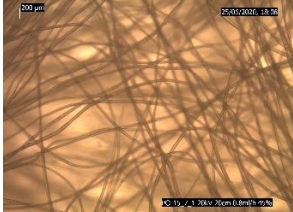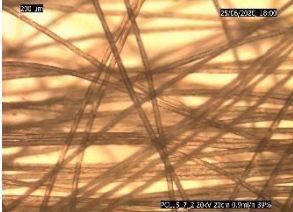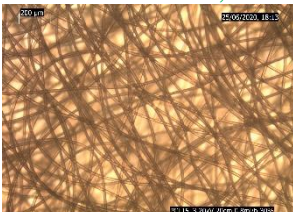
12.5 wt.%

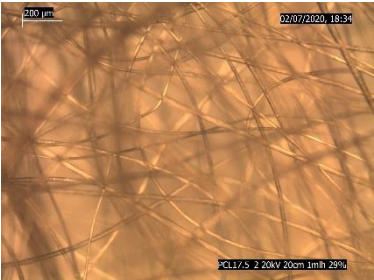| Voltage (KV)	Distance (cm)			
	10	15	17	20
20		12.5.2-0.7ml/h 31% 		12.5.1-0.7ml/h 31%
		12.5.5-0.7mlh 35% 		12.5.3-0.6ml/h 31%
		12.5.6-0.7mlh 35% 		12.5.4-0.8mlh 31%
		12.5.8-0.6mlh 36% 		12.5.7-0.6mlh 35%
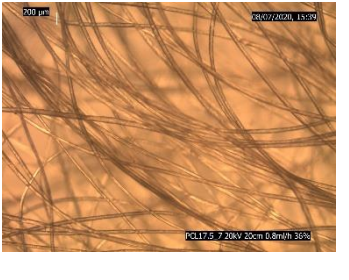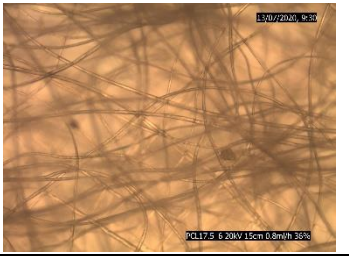
		12.5.9-0.5mlh 36%		12.5.11-0.6mlh 36%
		12.5.9-0.4mlh 36%		

15 wt.%

Voltage (KV)	Distance (cm)	
	15	**20**
20	15.8-0.8 mL/h, H 42% 	15.1-1 mL/h, H 30%
	15.9-0.7 mL/h, H 37% 	15.2-0.8 mL/h, H 30%
		15.4-0.8 mL/h, H 35%

		15.7-1-0.8 mL/h, H 45%
		15.7-2-0.9 mL/h, H 39%
		PCL15.3-0.8 mL/h, H 30%

17.5 wt.%

Voltage (KV)	Distance (cm)	
	15	**20**
20	17.5.3-1ml/h 29%	17.5.1-0.8ml/h 35%
	17.5.7-0.8ml/h 36%	17.5.2-1ml/h 29%
	17.5.6 – 0.8ml/h 36%	17.5.4-1ml/h 35%

		17.5.5- 0.8mlh 36%